IEEE Access
Multidisciplinary | Rapid Review | Open Access Journal

Received March 13, 2022, accepted March 28, 2022, date of publication April 4, 2022, date of current version April 15, 2022.

*Digital Object Identifier 10.1109/ACCESS.2022.3164515*

# Distributed Fusion of Optimally Quantized Local Tracker Estimates for Underwater Wireless Sensor Networks

**B. N. BALARAMI REDDY, (Graduate Student Member, IEEE), BETHI PARDHASARADHI, GUNNERY SRINATH, (Graduate Student Member, IEEE), AND PATHIPATI SRIHARI, (Senior Member, IEEE)**
ECE Department, National Institute of Technology Karnataka Surathkal, Surathkal, Mangalore 575025, India
Corresponding author: Pathipati Srihari (srihari@nitk.edu.in)

**ABSTRACT** Multi-sensor underwater surveillance has been a significant research problem for civilian and naval applications. Due to limited bandwidth considerations, the underwater wireless sensor networks (UWSNs) use measurement quantization to transmit information from individual sensors to the fusion center to perform centralized tracking/fusion. However, at the measurement level, quantization of azimuth information is complex due to its non-linear behavior. To address this problem, this paper proposes to perform the distributed tracking and quantizing the local estimates (state and covariance) to provide improved bandwidth and reduce computational load. The local tracker estimates the updated state and covariance of a target's time-varying dynamics in the given surveillance from the obtained measurements using extended Kalman filter (EKF) and global nearest neighbor (GNN) data association. The measurement model contains both detections of target and false alarms. This paper uses optimal quantization rather than linear quantization owing to its minimal bandwidth requirement. Once the quantized local tracks are obtained at the fusion center, these tracks are quantified using track-to-track association (T2TA) in the S-D assignment framework. The associated tracks are fused using correlation-free fusion algorithms like covariance intersect (CI), sampling covariance intersects (SCI), ellipsoidal intersect (EI), and arithmetic average (AA) algorithms to achieve the global track. The position root mean square error (PRMSE), bandwidth, and error ellipses are used to quantify the performance of the proposed framework. The simulation results show that the PRMSE of the optimally quantized fusion estimates yields good agreement with the unquantized method. Simulation results further reveals that, optimal quantization utilizes lower bandwidth compared to linear quantization. In addition, optimally quantized local estimates accomplishes promising covariance regions at the fusion center.

**INDEX TERMS** Correlation-free fusion, extended Kalman filter, state quantization, target tracking, track-to-track association.

## I. INTRODUCTION

Deployment of the large number of active and passive underwater sensors and their cooperative network is an emerging topic for both monitoring as well as target tracking in a given surveillance [1]. The sensor-to-sensor and sensors-to-fusion center data exchange is essential for centralized tracking/fusion. Observation of targets (maneuvering targets, autonomous vehicles, marine species, and other ocean resources [2]), with considerable implications in navigation, military, defense, disaster management, and other civilian applications [3] is a significant research problem during recent years. In the terrestrial scenario, communication between various sensors has been accomplished using radio frequency (RF) waves due to the high-frequency spectrum with good bandwidth for several wireless sensor networks applications. Due to forbidden RF wave propagation conditions in the underwater scenario, sensors establish communication among them using acoustic waves or light waves rather than radio waves. As a result, Underwater

The associate editor coordinating the review of this manuscript and approving it for publication was Juan A. Lara.

Wireless Sensor Networks (UWSN) provide limited available bandwidth compared to terrestrial Wireless Sensor Networks (WSN). Limited bandwidth is inadequate with regular information exchange between the sensors to perform error-free communications in multi-sensor multi-target applications in UWSNs. Therefore, it requires alternative solutions to address this important problem.

Quantization is a powerful tool to address the limited bandwidth problem within the given network with minimal information loss due to quantization error [4]. There are two types of quantization techniques: uniform and non-uniform quantization. Uniform or linear quantization is a simple and popular technique that has been employed to quantize the analog to digital conversion based on the assumption of linear levels and is predominately employed in various applications [4]. Apart from the linear quantization technique, an optimal quantization technique is proposed in the literature, in which the quantization is achieved with optimal quantization threshold levels [5]. Quantization is performed on received measurements in several application domains (data communications, wireless communications, and digital filtering etc.) to accommodate limited bandwidth requirements [6]–[11].

### A. RELATED WORK

In UWSN with limited bandwidth constraints, researchers propose quantizing the measurements and thereafter transmitting them to the fusion node to perform centralized tracking/fusion. Here, quantized measurements from multiple sensors are sent to the central fusion node to estimate the parameter of interests like position, velocity, and acceleration of the target directly at the fusion node. Sensor-centric data reduction for estimation with WSNs via censoring and quantization is proposed in [6]. A new distributed adaptive quantization system is presented in [7], in which each sensor node's quantizer threshold is dynamically adjusted based on previous transmissions from other sensor nodes. Besides, optimizing the quantizer under energy constraints is reported in [8]. In addition, multiple target tracking with quantized measurements in a Bayesian framework is presented in [9]. Moreover, the approximate minimum means square error (MMSE) approach for state estimation with the quantized measurements is presented in [10]. In a recent communication [11], a method for tracking the targets is proposed, which uses the readily updated optimum quantization thresholds based on real-time target states. The authors in [12] presented a quantizer with adaptive threshold levels. These adaptive threshold levels are determined by maximizing the entropy while considering the probability density function (pdf) of randomly selected measured signal amplitude. Thereafter, the particle filter is used in the fusion center for target tracking [12]. In another communication, localization using novel Bayesian compressed sensing framework with quantized received signal strength-based measurements is proposed in [13]. Further, to improve tracking accuracy, the optimal bit allocation method is deployed in [14]. The suggested optimal bit allocation approach [14] takes into account both node topology and sensor-to-target range. Furthermore, authors in [15] proposed switched quantizer-based event triggered-Kalman consensus filtering algorithm to overcome the limited bandwidth conditions in WSNs. It is evident from all the above literature, data fusion plays a significant role in combining the quantized measurements at the fusion center, coming from several sensors.

#### 1) TARGET TRACKING

Target tracking is one of the most important applications in WSN in which one or more sensor nodes monitor and report the time-varying kinematics of moving objects to the fusion center. The sensor measurements come from various places, including the targets of interest, intentional interference, clutter, etc. The fundamental goal of target tracking is to track the targets of interest by estimating the parameters such as position, velocity, acceleration, turn, intensity, etc. Filtering, data association, and track management are the fundamental blocks of a tracker. Under the principles of linearity and Gaussianity, the Kalman filter (KF) delivers the best estimate [16]. Converted Kalman filter, extended Kalman filter (EKF), cubature Kalman filter (CKF), unscented Kalman filter (UKF), Interactive multiple models (IMM), and particle Kalman filter (PKF), among others, are frequently employed to address non-linearity issues in target tracking [17]. Target tracOn the other hand, data association is performed by using classical methods such as nearest neighbor (NN) and global nearest neighbor (GNN) that consider only a single measurement out of all available measurements that fall within the validation gate [18]. The weighted summation of all measurements within the validation gate is utilized in the probabilistic data association (PDA) based technique [19]. Under the assumption of propagating all hypotheses into tracks, the best strategy for target tracking was demonstrated by using a multiple hypothesis tracker (MHT) [20]. Track management methods such as logic-based track maintenance and quality-based track maintenance are widely used [21]. Single or multiple sensors can track targets in either a centralized or distributed framework. A novel data association solution for multi-object pedestrian tracking in thermal images is proposed in [22]. The authors in [23] proposed point-track-transformer (PTT) module to focus on the important features of objects while tracking.

The track-to-track association (T2TA) is an essential component in distributed target tracking since it distinguishes and assigns the tuples that belong to the same targets [24]. The global estimates are obtained by fusing the tuples of tracks reported by the T2TA block.

#### 2) SENSOR FUSION

The sensor fusion is a powerful technique to fuse multiple sensor data to produce the best estimates for a given parameter of interest [25]. Data fusion finds a wide range of applications in many fields like Wireless sensor networks (WSN), Underwater Wireless sensor networks (UWSN),

robotics, control engineering, medical electronics etc. [26], [27]. By taking the advantage of radial basis function (RBF) neural network with error state KF, a novel multi-sensor fusion algorithm that improves state estimation for underwater vehicle localization is proposed in [28]. Further, data fusion is broadly categorized into centralized and distributed fusion. In the multi-sensor scenario, distributed fusion is popular over centralized structure because of the distribution of computation load among multiple sensor nodes and simultaneously reducing the bandwidth requirement at the central fusion node [29]. The centralized fusion requires higher computational requirements, owing to its ability to fuse all the available measurements. In addition, track-to-track fusion (T2TF) approaches are broadly divided into two types: correlation-free and correlation-based fusion methods [30]. The correlation-based fusion technique requires the exact cross covariances among the local tracks of the same target. As a result, a large amount of information exchange between the fusion center (FC) and the local trackers takes place [31]. In theory, information matrix fusion (IMF) or centralized tracking yields the estimate/ fused track [17]. On the other hand, the correlation-free-based fusion algorithms require no correlation information while fusing the estimates at the fusion center. The correlation free fusion methods include covariance intersect (CI) [32], sampling covariance intersect (SCI) [33], ellipsoidal intersect (EI) [34], arithmetic average (AA) [35], and others. Furthermore, by approximating the intersection region of individual ellipsoids, the CI, SCI, and EI methods provide the fused estimate. However, AA provides the fused estimate by averaging technique [35], [36]. The CI and EI methods provide good performance for two sensor-based fusion. In contrast, the AA provides the conservativeness of fused estimate. Alternatively, the SCI provides a better-fused estimate with more flexibility in information sharing across a distributed sensor network when fusing many data sources.

In the above literature, most of the research articles [6], [9]–[13], [37] concentrate on measurement quantization and addressed the tracking/fusion problem under low bandwidth scenarios. Further, most of the contributions considers range information, which is easy to quantize. However, one of the investigations with azimuth quantization [38] clearly shows that the quantization of azimuth information is complex due to its non-linear behavior and requires more quantization levels, which in turn increases the required bandwidth [38]. Further, limited amount of contributions were focused on quantization of state and covariance in distributed sensor scenario. Therefore, there is a strong need to carryout research investigation in this direction to provide efficient and alternative solution to this problem. This motivated us to consider the problem in state (cartesian coordinates) quantization rather than measurement (polar coordinates) quantization. The state quantization is more feasible in real-time because of its linear relationship. Moreover, centralized fusion is complex and computationally expensive. This paper considers distributed tracking. Every sensor is associated with a local tracker module to provide the local estimates. Lloyd's based optimal quantization is used to quantize the local estimates. The association of the tracks pertaining to the same origin is resolved using track-to-track association from all the available tracks. These associated local estimates are then used to perform the fusion to obtain the global estimates. Since the correlation information is not available in distributed fusion [31], this paper utilizes the correlation-free fusion algorithms.

The article's main contributions are

1) The local estimator is developed based on the EKF and GNN framework. Two quantization techniques, namely linear and optimal quantization, are utilized to quantize the local estimates.
2) The quantized local estimates are associated using track-to-track association in the S-D assignment framework.
3) The associated local tracks are fused with fusion algorithms like CI, EI, SCI, and AA to examine the quantization performance on fused tracks.

The organization of the paper is as follows. The problem formulation is outlined in Section II. Section III presents distributed tracking and state quantization. The following Section IV presents the track-to-track association and fusion. Further, Section V deals with the results and discussion. Finally, Section VI concludes the paper.

## II. PROBLEM FORMULATION

Consider a problem of underwater distributed target tracking with $S$ number of sensors. Each sensor is associated with its local tracker. The sensor static locations are $\{\mathbf{x}_i\}_{i=1}^{S}$. Let the number of time-varying targets be $N$ and their positions are represented by $\{\mathbf{x}_j\}_{j=1}^{N}$ as depicted in Fig. 1. The sensors acquire measurements as range and azimuth about the targets. Based on the collected measurements, the local tracker estimates the state and covariance of targets. Traditionally, the measurements are quantized and sent to the fusion node [6], [9]–[13], [37], [38]. The Local estimates are quantized and then sent to the fusion node to obtain fused/global estimates. The time-varying dynamics of the target is represented and follows

$$\mathbf{x}(k+1) = F(k)\mathbf{x}(k) + v(k), \tag{1}$$

where $\mathbf{x}$ is the state of the target consists of position and corresponding velocity components i.e., $\mathbf{x} = \begin{bmatrix} x & \dot{x} & y & \dot{y} \end{bmatrix}'$. $F(k)$ is the state transition matrix follows models like constant velocity (CV), constant acceleration(CA), and constant turn (CT) etc. The $v(k)$ is a process noise follows white Gaussian distribution with covariance $Q(k)$. The sensor $i$ receives a measurement set $\mathbf{Z}_i(k)$, which contains measurements originated from targets and false alarms within the surveillance region.

$$\mathbf{Z}_i(k) = \left\{ \mathbf{z}_i^1(k), \mathbf{z}_i^2(k), \cdots, \mathbf{z}_i^{n_k}(k) \right\}. \tag{2}$$

Here, $n_k$ represents total number of measurements at time $k$. The measurement pertaining to target originated is designated

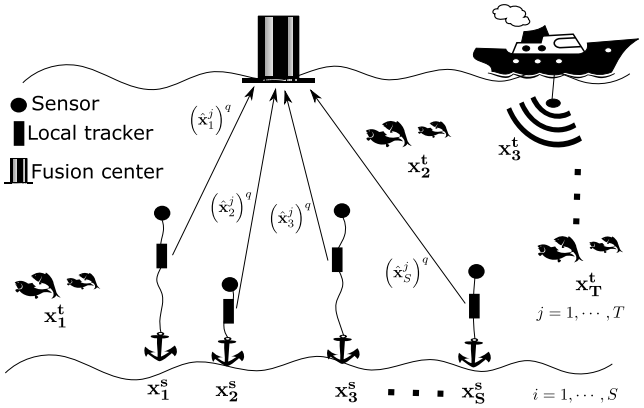


**FIGURE 1.** Under water multi sensor multi target scenario (The transfer of data from local tracker to fusion node is given in black arrows).

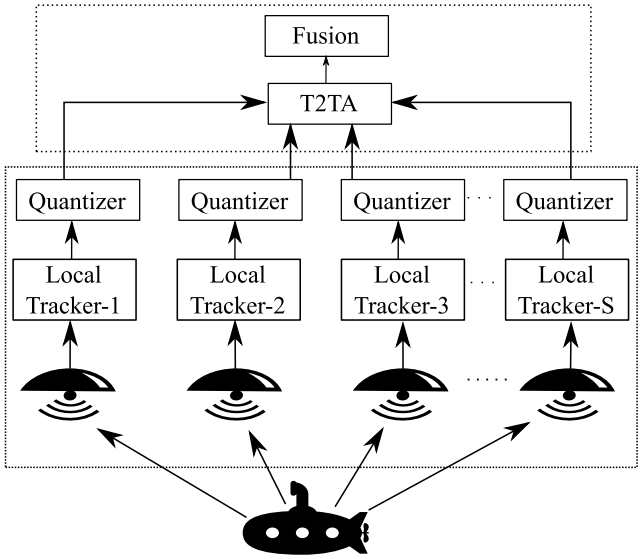


**FIGURE 2.** Block diagram representation of proposed methodology.

as

$$\mathbf{z}_i^j(k) = h(\mathbf{x}_i^j(k)) + w(k), \tag{3}$$

where $w$ is assumed to be white Gaussian noise with measurement covariance $R(k)$. The $h(\cdot)$ represents the non-linear relation between the measurement space and the state space. The false alarms are assumed to be independent and follows Poisson distribution, given by

$$P(n_{FA}) = \frac{\exp(-N_p)(N_p)^m}{m!}, \tag{4}$$

where $N_p$ is the number of cells under consideration over a volume $V$. The spatial density of false alarm is given by

$$\lambda = \frac{N_p}{V}. \tag{5}$$

The probability of having $n_k$ measurements originated from a given volume $V$ is

$$P(n_k) = \begin{cases} (1 - P_D)\mu(0); & n_k = 0, \\ (1 - P_D)\mu(n_k) + (P_D)\mu(n_k); & n_k > 0. \end{cases} \tag{6}$$

Here, $P_D$ is probability of target detection. The measurement $\mathbf{z}_i^j(k)$ consists of range and azimuth between sensor $i$ and target $j$, and are characterized as

$$r_i^j = \sqrt{\left(x_i^s - x_j^t\right)^2 + \left(y_i^s - y_j^t\right)^2} + \mathcal{N}(0, \sigma_r^2) \tag{7}$$

and

$$\theta_i^j = \tan^{-1}\left(\frac{y_i^s - y_j^t}{x_i^s - x_j^t}\right) + \mathcal{N}(0, \sigma_\theta^2) \tag{8}$$

respectively. Here $x, y$ are the 2-D Cartesian co-ordinates. $\mathcal{N}(\cdot)$ represent Gaussian pdf, $\sigma_r$ and $\sigma_\theta$ are the variances of range and theta respectively.

Using the measurement set $\mathbf{Z}_i(k)$, the sensor estimates the target dynamics to acquire updated state and covariance $\left\{\hat{\mathbf{x}}_i^j(k), P_i^j(k)\right\}_{j=1}^N$. These updated state and covaraince information is quantized as $\left\{\left(\hat{\mathbf{x}}_i^j\right)^q(k), \left(P_i^j\right)^q(k)\right\}_{j=1}^N$ and transmitted to fusion node as shown in Fig. 1. In this problem, one needs to investigate the type of quantization required (linear or non-linear) and the minimum number of quantization levels that are required to achieve a comparable PRMSE as that of without quantization method. Moreover, in multi-target multi-sensor scenario, before performing the fusion, one needs to associate the tracks pertain to the same origin. Since the tracks are independent there is a need to perform the correlation-free based fusion.

## III. DISTRIBUTED TRACKING AND STATE QUANTIZATION

In this section, first we obtained the state and covariance estimates from the observations of the sensors in a EKF and GNN association framework. The local estimates are quantized by using linear and non-linear quantization techniques. The processing steps are represented in Fig. 2, and operation of the individual blocks are explained below.

### A. DISTRIBUTED TRACKER

The individual sensor in a distributed sensor network contains a local tracker to process the observations. The Kalman filter gives an optimal solution under the linear Gaussian assumption. Due to the non-linearity relationship exists among the measurements and state, the measurements are filtered using EKF. From the prior state and covariance at $k-1$, the EKF predicts and updates the state and covariance using all the available measurements till $k$. Let $\mathbf{x}_i^j(k)$ be the state of $j^{\text{th}}$ target at $k^{\text{th}}$ scan for the sensor $i$. Then the predicted state is given by

$$\hat{\mathbf{x}}_i^j(k+1|k) = F^j \hat{\mathbf{x}}_i^j(k|k), \tag{9}$$

where $\hat{\mathbf{x}}_i^j(k|k)$ is the previous state of $j^{\text{th}}$ target pertaining to $i^{\text{th}}$ sensor. The $F_i^j$ represents the state transition matrix, which follows either CV, CT, or CA models [16]. Let, $P_i^j$ be the

covariance matrix corresponding to the state $\hat{\mathbf{x}}_i^j$. Then, the predicted covariance is

$$P_i^j(k+1|k) = F_i^j P_i^j(k|k) F_i^{j'} + Q_i^j(k+1). \tag{10}$$

Here, $(\cdot)'$ indicates the transposition operation and $Q$ is noise covariance matrix. Similarly, the measurement prediction is given by

$$\hat{\mathbf{z}}_i^j(k+1) = H_i^j(k+1)\hat{\mathbf{x}}_i^j(k+1|k). \tag{11}$$

Here, $H_i^j$ is linear measurement transition matrix obtained from first order Taylor's expansion, represented as

$$H_i^j = \begin{bmatrix} \frac{\partial r_i^j}{\partial x_j} & \frac{\partial r_i^j}{\partial \dot{x}_j} & \frac{\partial r_i^j}{\partial y_j} & \frac{\partial r_i^j}{\partial \dot{y}_j} \\ \frac{\partial \theta_i^j}{\partial x_j} & \frac{\partial \theta_i^j}{\partial \dot{x}_j} & \frac{\partial \theta_i^j}{\partial y_j} & \frac{\partial \theta_i^j}{\partial \dot{y}_j} \end{bmatrix}. \tag{12}$$

The elements of $H_i^j$ matrix are obtained from application of partial derivatives to range and azimuth with respect to coordinates is as follows

$$\begin{aligned} \frac{\partial r_i^j}{\partial x_j} &= \frac{x_j - x_i}{\sqrt{(x_i - x_j)^2 + (y_i - y_j)^2}} \\ \frac{\partial r_i^j}{\partial y_j} &= \frac{y_j - y_i}{\sqrt{(x_i - x_j)^2 + (y_i - y_j)^2}} \\ \frac{\partial \theta_i^j}{\partial x_j} &= \frac{y_i - y_j}{(x_i - x_j)^2 + (y_i - y_j)^2} \\ \frac{\partial \theta_i^j}{\partial y_j} &= \frac{x_j - x_i}{(x_i - x_j)^2 + (y_i - y_j)^2} \end{aligned} \tag{13}$$

and rest of the partial differentials are zero. The innovation vector $\tilde{\mathbf{z}}_i^j(k+1)$ is designated as

$$\tilde{\mathbf{z}}_i^j(k+1) = \mathbf{z}_i^j(k+1) - \hat{\mathbf{z}}_i^j(k+1), \tag{14}$$

where $\mathbf{z}_i^j(k+1)$ is the associated measurement. One measurement from the set $\mathbf{z}_i(k+1)$ is generally considered to compute the innovation. At time k, $T_k$ tracks are evolved, these tracks are to be associated with $\mathbf{z}_i(k+1)$ measurements.

In multiple target scenario, the association is formulated as an optimization problem represented as

$$C(k+1|a(k+1)) = \sum_{i=0}^{n_{k+1}} \sum_{t=0}^{T_k} a(k+1,i,t)c(k+1,i,t) \tag{15}$$

subjected to

$$\begin{aligned} &\sum_{i=0}^{n_{k+1}} a(k+1,i,t) = 1, \quad t = 1,2,\ldots,T_k \\ &\sum_{t=0}^{T_k} a(k+1,i,t) = 1, \quad i = 1,2,\ldots,n_{k+1} \end{aligned} \tag{16}$$

where $c(k+1,i,t)$ is the cost of the assignment. Further, $a(k+1,i,t)$, $n_{k+1}$ and $T_k$ are the cardinalities of the measurement and track sets, respectively. A binary assignment variable $a(k+1,i,t)$ is defined such that

$$a(k+1,i,t) = \begin{cases} 1; & i^{\text{th}} \text{ measurement is assigned to track } t \\ 0; & \text{otherwise} \end{cases} \tag{17}$$

The updated state and covariance of $j^{\text{th}}$ target is given by

$$\hat{\mathbf{x}}_i^j(k+1|k+1) = \hat{\mathbf{x}}_i^j(k+1|k) + K_i^j(k+1)\tilde{\mathbf{z}}_i^j(k+1) \tag{18}$$

and

$$\begin{aligned} &P_i^j(k+1|k+1) \\ &\quad = P_i^j(k+1|k) - K_i^j(k+1)H_i^j(k+1)K_i^{j'}(k+1), \end{aligned} \tag{19}$$

respectively. Where $K$ is KF gain, which is given as

$$K_i^j(k+1) = P_i^j(k+1|k)H_i^{j'}(k+1)S^{-1}, \tag{20}$$

where

$$S = H_i^j(k+1)P_i^j(k+1|k)H_i^{j'}(k+1) + R_i^j. \tag{21}$$

The track maintenance module is a combination of initiation, confirmation, and deletion of tracks [39]. Initially, each detection made from the sensor observations is represented as an individual tentative track. The tentative tracks are confirmed or deleted based on the logic based track management.

- To initiate the track: If at least $M_{\text{initiation}}$ measurements are associated in the last $N_{\text{initiation}}$ measurement sets, establish a track and label it tentatively; otherwise, ignore.
- For a tentative track: If at least $M_{\text{tentative}}$ measurements are associated with the track from the latest $N_{\text{tentative}}$ measurement sets, upgrade it as confirmed; else, discard that track.
- For a confirmed track: If at least $M_{\text{confirmed}}$ measurements are associated with the track from the last $N_{\text{confirmed}}$ measurement sets, maintain the confirmed status. Otherwise, delete the track.

We have applied quantization on local estimates before sending them to the fusion node. The following subsection presents the quantization methods considered to quantize the state information.

### B. QUANTIZATION OF LOCAL ESTIMATES

This subsection briefly describes the quantization of local estimates. Let the quantized local estimates of state and covariance are represented as

$$\begin{aligned} (\hat{\mathbf{x}}_i^j)^q &= \mathcal{Q}(\hat{\mathbf{x}}_i^j), \\ (P_i^j)^q &= \mathcal{Q}(P_i^j). \end{aligned} \tag{22}$$

Here $\mathcal{Q}(\cdot)$ represents the quantization of the parameter of interest. This quantization can be either linear or

non-linear [4]. The total available estimates from all local estimates at the fusion center is $\hat{\mathbf{X}}$, designated as

$$\hat{\mathbf{X}} = \left\{ \left\{ \hat{\mathbf{x}}_i^j \right\}_{i=1}^{S} \right\}_{j=1}^{N}. \tag{23}$$

Here $N$ and $S$ represent the number of targets in the given surveillance and the number of sensors employed, respectively.

#### 1) LINEAR QUANTIZATION

In linear quantization, the uniform step size ($\nabla$) is calculated by considering minimum and maximum values of the local estimates, given by

$$\nabla_X = \frac{\zeta_{\max} - \zeta_{\min}}{L_X}, \tag{24}$$

$$\nabla_P = \frac{\eta_{\max} - \eta_{\min}}{L_P}, \tag{25}$$

where $\zeta$ is an element from the state vector $\mathbf{x}$, and $\eta$ is an element from the covariance matrix $P$. Therefore, $\{\zeta_{\max}, \zeta_{\min}\}$, and $\{\eta_{\max}, \eta_{\min}\}$ are the maximum, minimum value of the local state estimates and covariances, respectively. Further, the $L_X$, $L_P$ are the number of quantization levels in state and covariance estimates respectively. The partition levels are selected based on the step size defined in (24).

$$\begin{aligned}
\mathcal{Q}_1 &= \{\zeta : -\infty < \zeta \le \zeta_1 = \zeta_{\min}\} \\
\mathcal{Q}_2 &= \{\zeta : \zeta_1 < \zeta \le \zeta_2 = (\zeta_{\min} + \nabla)\} \\
&\vdots \\
\mathcal{Q}_{\nu-1} &= \{\zeta : \zeta_{\nu-2} < \zeta \le \zeta_{\nu-1}\} \\
\mathcal{Q}_{\nu} &= \{\zeta : \zeta_{\nu-1} < \zeta \le \zeta_{\nu} = \zeta_{\max}\}
\end{aligned} \tag{26}$$

Finally, the quantized values $q_\alpha$ for the relevant partition levels $\mathcal{Q}_\alpha$ are picked from the code-book $C_\alpha$. Where $\alpha = 1, 2, \cdots, \nu$. The appropriate partition's code-book values are chosen as floor, mid, or ceiling values [5]. The code-book values in this paper are based on the floor values of the respective part. i.e.,

$$\zeta_\alpha^q = \{C_\alpha = \text{floor}\,(\mathcal{Q}_\alpha)\}. \tag{27}$$

The similar analogy holds for the covariance and it is designated as $\eta_\beta^q = \{C_\beta = \text{floor}\,(\mathcal{Q}_\beta)\}$, where $\beta$ is the number of levels pertaining to covariance. In Linear quantization, data loss occurs as a result of quantization error. In order to reduce the quantization error, the optimal quantization is adopted. The optimal quantization is described in the following subsection.

#### 2) OPTIMAL QUANTIZATION

To accomplish good quantization levels with minimum quantization error, Lloyd [5] approach is adapted. Lloyd's approach for determining the optimum quantization levels is based on the least-square minimization of quantization error $\varepsilon$, defined as

$$\varepsilon = \sum_{\alpha=1}^{\nu} \int_{\mathcal{Q}_\alpha} \left(\zeta_\alpha^q - \zeta\right)^2 df(\zeta), \tag{28}$$

where $\zeta_\alpha^q$ and $\mathcal{Q}_\alpha$ represent quantized values and fixed pre-assigned sets. The uniquely determined optimum quanta to employ with a given partition $\{\mathcal{Q}_\alpha\}$, to yield the smallest qunatization error $\varepsilon$ as defined in (28), is given by

$$\zeta_\alpha^q = \frac{\int_{\mathcal{Q}_\alpha} \zeta \, df(\zeta)}{\int_{\mathcal{Q}_\alpha} df(\zeta)} \tag{29}$$

Further, with the provided quantization levels, the optimum partition values are given by

$$\begin{aligned}
\mathcal{Q}_1 &= \{\zeta : -\infty < \zeta \le \zeta_1\} \\
\mathcal{Q}_2 &= \{\zeta : \zeta_1 < \zeta \le \zeta_2\} \\
&\vdots \\
\mathcal{Q}_{\nu-1} &= \{\zeta : \zeta_{\nu-2} < \zeta \le \zeta_{\nu-1}\} \\
\mathcal{Q}_{\nu} &= \{\zeta : \zeta_{\nu-1} < \zeta \le \zeta_{\nu}\}
\end{aligned} \tag{30}$$

where $\{\zeta_\alpha\}$ denotes the end points and are represented as

$$\zeta_{\nu-1} = \frac{1}{2}\left(\zeta_{\nu-1}^q + \zeta_\nu^q\right) \tag{31}$$

Similarly, the same set of equations are considered for quantization of covariances with $\eta_{\nu-1} = \frac{1}{2}\left(\eta_{\nu-1}^q + \eta_\nu^q\right)$. All the elements of state & covariance are quantized and finally attained $\hat{\mathbf{x}}^q$ and $P^q$ values.

## IV. TRACK-TO-TRACK ASSOCIATION AND FUSION

The quantized state & covariance information is transferred to fusion node to obtain the fused estimates. However, to determine the fused estimate, one needs to distinguish the individual tracks pertaining to the same target and this is carried-out using T2TA. The associated tracks are then sent to the fusion node to estimate the fused track. This is illustrated in the Fig. 2.

### A. TRACK-TO-TRACK ASSOCIATION (T2TA)

In the form of target estimates $\hat{\mathbf{x}} = \left\{ \left\{ \left(\hat{\mathbf{x}}_i^q\right)^{n_i} \right\}_{i=1}^{S} \right\}_{n_j=1}^{M}$, the $S$ sensors will have their own number of quantized tracks having errors distributed as zero-mean Gaussian with covariance $\left(P_i^q\right)^{n_i}$. The sensor number is represented by $i = 1, 2, \ldots, S$ and the number of tracks on each sensor is represented by $n_i = 1, 2, \ldots, M$. To locate the tracks that are originated from the same target, use the likelihood ratio test, which is defined by

$$\chi\left(\mathcal{H}^1_{n_1,n_2,\ldots,n_S} : \mathcal{H}^0_{n_1,n_2,\ldots,n_S}\right) = \frac{\mathbf{L}\left(\mathcal{H}^1_{n_1,n_2,\ldots,n_S}\right)}{\mathbf{L}\left(\mathcal{H}^0_{n_1,n_2,\ldots,n_S}\right)}, \tag{32}$$

where $\mathbf{L}(\mathcal{H}^1_{n_1,n_2,\ldots,n_S})$ represents the likelihood hypothesis for tracks with the same target origin and $\mathbf{L}(\mathcal{H}^0_{n_1,n_2,\ldots,n_S})$ represents the likelihood hypothesis for tracks with different target origins. The following is used to calculate the likelihood hypothesis of tracks with a shared origin:

$$\mathbf{L}\left(\mathcal{H}^1_{n_1,n_2,\ldots,n_S}\right) = p\left(\left(\hat{\mathbf{x}}^q_S\right)^{n_S},\ldots,\left(\hat{\mathbf{x}}^q_1\right)^{n_1}|\mathcal{H}^1_{n_1,n_2,\ldots,n_S}\right) \tag{33}$$

The (33) can alternatively be expressed with the first sensor's track estimate, which is provided by

$$\mathbf{L}\left(\mathcal{H}^1_{n_1,n_2,\ldots,n_S}\right) = p\left(\left(\hat{\mathbf{x}}^q_S\right)^{n_S},\ldots,\left(\hat{\mathbf{x}}^q_2\right)^{n_2}|\mathcal{H}^1,\left(\hat{\mathbf{x}}^q_1\right)^{n_1}\right) \times p\left(\left(\hat{\mathbf{x}}^q_1\right)^{n_1}|\mathcal{H}^1\right) \tag{34}$$

The $p\left(\left(\hat{\mathbf{x}}^q_1\right)^{n_1}|\mathcal{H}^1\right)$ independent of $\mathcal{H}^1_{n_1,n_2,\ldots,n_S}$, hence it can be relaxed. In addition, it is assumed to be a uniform distribution, which is reasonable in the absence of data. i.e.,

$$p\left(\left(\hat{\mathbf{x}}^q_1\right)^{n_1}|\mathcal{H}^1_{n_1,n_2,\ldots,n_S}\right) = p\left(\left(\hat{\mathbf{x}}^q_1\right)^{n_1}\right) = \frac{1}{C} \tag{35}$$

Using (35), (34) can be written as

$$\mathbf{L}\left(\mathcal{H}^1_{n_1,n_2,\ldots,n_S}\right) = \frac{1}{C}p\left(\left(\hat{\mathbf{x}}^q_S\right)^{n_S},\ldots,\left(\hat{\mathbf{x}}^q_2\right)^{n_2}|\mathcal{H}^1,\left(\hat{\mathbf{x}}^q_1\right)^{n_1}\right) \tag{36}$$

Consider the case of two sensors $(i, j)$ with two common origin tracks $(n_i, n_j)$. If the tracks $\left(\hat{\mathbf{x}}^q_i\right)^{n_i}$, $\left(\hat{\mathbf{x}}^q_j\right)^{n_j}$ at sensor $i$, sensor $j$ result from the same target under the Gaussian assumption, the likelihood function of the two tracks is given by [24]

$$\mathbf{L}(\mathcal{H}_{n_1,n_2}) = \frac{1}{C}\mathcal{N}(\mathbf{x};\bar{\mathbf{x}},P) \tag{37}$$

where

$$\begin{aligned}\mathbf{x} &= \left(\hat{\mathbf{x}}^q_i\right)^{n_i} - \left(\hat{\mathbf{x}}^q_j\right)^{n_j},\\ \bar{\mathbf{x}} &= 0,\\ P &= \left(P^q_i\right)^{n_i} + \left(P^q_j\right)^{n_j} - \left(\left(P^q_{i,j}\right)^{n_i,n_j}\right)'.\end{aligned} \tag{38}$$

Here $\mathcal{N}(\mathbf{x};\bar{\mathbf{x}},P)$ denotes a Gaussian distribution of variable $\mathbf{x}$ with $\bar{\mathbf{x}}$, $P$ as mean and covariance, respectively.

The generalised likelihood function of all the common tracks (error $= 0$), $n_1, n_2, \ldots, n_S$ for all $S$ sensors is designated as, (similar to the expression in (37)):

$$\mathbf{L}\left(\mathcal{H}^1_{n_1,n_2,\ldots,n_S}\right) = \frac{1}{C}\mathcal{N}\left(\hat{\mathbf{x}}^q;0,P^q\right), \tag{39}$$

where

$$\hat{\mathbf{x}}^q = \left[\tilde{\mathbf{x}}^q_{21},\quad \tilde{\mathbf{x}}^q_{31},\quad \ldots,\quad \tilde{\mathbf{x}}^q_{S1}\right]', \tag{40}$$

where $\tilde{\mathbf{x}}^q_{ij}$ is the difference between the quantized state estimates obtained from the same target at $i^{th}$ and $j^{th}$ sensors, as determined by

$$\tilde{\mathbf{x}}^q_{ij} = \left(\hat{\mathbf{x}}^q_i\right)^{n_i} - \left(\hat{\mathbf{x}}^q_j\right)^{n_j}. \tag{41}$$

The trace of $P^q$ is given by

$$\begin{aligned}P^q_{i-1,i-1} &= \mathrm{E}\left[\left(\tilde{x}^q_{i1}\right)\left(\tilde{x}^q_{i1}\right)'|\mathcal{H}^1_{n_1,n_2,\ldots,n_S}\right]\\ &= \left(P^q_1\right)^{n_1} + \left(P^q_i\right)^{n_i} - \left(P^q_{1,i}\right)^{n_1,n_i} - \left(\left(P^q_{1,i}\right)^{n_1,n_i}\right)'\\ &\quad i = 2,\ldots,S,\end{aligned} \tag{42}$$

where $\tilde{\mathbf{x}}^q_{ij}$ is defined in (41), and E represents the expectation operation.

The $P^q$ diagonal elements are given by

$$\begin{aligned}P^q_{i-1,j-1} &= \mathrm{E}\left[\left(\tilde{x}^q_{i1}\right)\left(\tilde{x}^q_{j1}\right)'|\mathcal{H}^1_{n_1,n_2,\ldots,n_S}\right]\\ &= \left(P^q_1\right)^{n_1} - \left(P^q_{1,j}\right)^{n_1,n_j} - \left(\left(P^q_{1,i}\right)^{n_1,n_i}\right)'\\ &\quad + \left(P^q_{i,j}\right)^{n_i,n_j} \quad i,j = 2,\ldots,S\end{aligned} \tag{43}$$

The likelihood hypothesis of tracks with distinct target origins follows the same process as (39), and is represented as

$$\begin{aligned}&\mathbf{L}\left(\mathcal{H}^0_{n_1,n_2,\ldots,n_S}\right)\\ &= p\left(\left(\hat{\mathbf{x}}^q_S\right)^{n_S},\ldots,\left(\hat{\mathbf{x}}^q_2\right)^{n_2}|\mathcal{H}^0,\left(\hat{\mathbf{x}}^q_1\right)^{n_1}\right)p\left(\left(\hat{\mathbf{x}}^q_1\right)^{n_1}|\mathcal{H}^0\right)\\ &= \prod_{i=2}^{S} p\left(\left(\hat{\mathbf{x}}^q_i\right)^{n_i}|\mathcal{H}^0,\left(\hat{\mathbf{x}}^q_1\right)^{n_1}\right)p\left(\left(\hat{\mathbf{x}}^q_1\right)^{n_1}|\mathcal{H}^0\right)\end{aligned} \tag{44}$$

The $p\left(\left(\hat{\mathbf{x}}^q_1\right)^{n_1}|\mathcal{H}^0_{n_1,n_2,\ldots,n_S}\right)$ is considered to be a diffuse prior, similar to (35), given by

$$p\left(\left(\hat{\mathbf{x}}^q_1\right)^{n_1}|\mathcal{H}^0_{n_1,n_2,\ldots,n_S}\right) = p\left(\left(\hat{\mathbf{x}}^q_1\right)^{n_1}\right) = \frac{1}{C}, \tag{45}$$

In the state space with the spatial density $\lambda$, $p\left(\left(\hat{\mathbf{x}}^q_S\right)^{n_S},\ldots,\left(\hat{\mathbf{x}}^q_2\right)^{n_2}|\mathcal{H}^0,\left(\hat{\mathbf{x}}^q_1\right)^{n_1}\right)$ is assumed to follow a Poisson distribution. As a result, (44) can be expressed using (45) as,

$$\mathbf{L}\left(\mathcal{H}^0_{n_1,n_2,\ldots,n_S}\right) = \frac{1}{C}\lambda^{S-1}. \tag{46}$$

Finally, the likelihood ratio test is calculated using the equations (32), (39) and (46).

$$\chi(\mathcal{H}^1_{n_1,n_2,\ldots,n_S}:\mathcal{H}^0_{n_1,n_2,\ldots,n_S}) = \frac{\mathcal{N}\left(\hat{\mathbf{x}}^q;0,P^q\right)}{\lambda^{S-1}}. \tag{47}$$

Let's define the track-to-track assignment procedure for T2TA, which involves assigning the $S_i$ tracks generated by $S$ sensors that represent the same target. To do so, create a binary assignment variable.

$$\psi_{i_1,i_2,\ldots,i_S} = \begin{cases}1 & \text{tracks } i_1, i_2, \ldots, i_S \text{ from same target}\\ 0 & \text{from different target}\end{cases} \tag{48}$$

The constrained optimization problem below yielded the multidimensional (S-D) track to track assignment algorithm for determining the most likely hypothesis,

$$\min_{\psi_{i_1,i_2,\ldots,i_S}} \sum_{i_1=0}^{M_1}\sum_{i_2=0}^{M_2}\cdots\sum_{i_S=0}^{M_S} c_{i_1,i_2,\ldots,i_S}\psi_{i_1,i_2,\ldots,i_S} \tag{49}$$

subject to

$$\begin{aligned}
\sum_{i_2=0}^{M_2}\cdots\sum_{i_S=0}^{M_S}\psi_{j,i_2,\ldots,i_S} &= 1, \quad j=1,2,\ldots,M_1\\
\sum_{i_1=0}^{M_1}\sum_{i_3=0}^{M_3}\cdots\sum_{i_S=0}^{M_S}\psi_{i_1,j,i_3,\ldots,i_S} &= 1, \quad j=1,2,\ldots,M_2\\
&\vdots\\
\sum_{i_1=0}^{M_1}\cdots\sum_{i_{S-1}=0}^{M_{S-1}}\psi_{i_1,\ldots,i_{S-1}} &= 1, \quad j=1,2,\ldots,M_S
\end{aligned} \tag{50}$$

and

$$\begin{aligned}
&\psi_{i_1,\ldots,i_S}\in\{0,1\},\\
&i_1=0,1,\ldots,M_1,\\
&\vdots\\
&i_S=0,1,\ldots,M_S.
\end{aligned} \tag{51}$$

It is possible to calculate the cost function $c_{i_1,i_2,\ldots,i_S}$ in (49) as follows:

$$c_{i_1,i_2,\ldots,i_S} = -\ln\chi(\mathcal{H}^1:\mathcal{H}^0), \tag{52}$$

where $\chi(\mathcal{H}^1:\mathcal{H}^0)$ is the probability ratio as stated in (47).

### B. FUSION

In an underwater distributed environment, the individual sensor nodes operate independently. It is challenging to obtain correlation information among the sensors. So, this paper considers the correlation free fusion algorithms available in the literature, which are used at the fusion centre to produce consistent results in distributed sensor networks. They are listed as follows:

#### 1) COVARIANCE INTERSECTION (CI) ALGORITHM

The CI method combines the estimates from available state and covariances with unknown correlations by considering the covariances are independent. At the fusion node, assume $\hat{\mathbf{x}}_1^q$ and $\hat{\mathbf{x}}_2^q$ are two quantized state estimates and $P_1^q$ and $P_2^q$ are two quantized covariances. The CI algorithm [32] fuses the incoming estimates and provides new fused estimates, which is independent of unknown correlations.

The fused estimates of state $\left(\hat{\mathbf{x}}_f\right)$ and covariance $(P_f)$ from the CI algorithm are as follows,

$$(P_f)_{CI}^{-1} = \omega(P_1^q)^{-1} + (1-\omega)(P_2^q)^{-1}, \tag{53}$$

$$(\hat{\mathbf{x}}_f)_{CI} = (P_f)_{CI}\left(\omega(P_1^q)^{-1}\hat{\mathbf{x}}_1^q + (1-\omega)(P_2^q)^{-1}\hat{\mathbf{x}}_2^q\right). \tag{54}$$

Here, $\omega\in[0,1]$ is the parameter needs to be optimized [40]. Let $C$ be a cost function, which is to be selected arbitrarily and optimized value $(\omega)$ for CI can be found by the following equation.

$$\omega^* = \arg\min_{\omega}\left\{C((\omega(P_1^q)^{-1} + (1-\omega)(P_2^q)^{-1})^{-1})\right\}. \tag{55}$$

#### 2) ELLIPSOID INTERSECTION ALGORITHM

To improve the fusion accuracy of quantized state and covariance estimates with unknown correlations in two sensor case, ellipsoid intersection algorithm is generally deployed.

The fused estimates of state and covariance from EI algorithm [34] are as follows,

$$(P_f)_{EI}^{-1} = (P_1^q)^{-1} + (P_2^q)^{-1} - \Gamma^{-1} \tag{56}$$

$$(\hat{\mathbf{x}}_f)_{EI} = (P_f)_{EI}\left((P_1^q)^{-1}\hat{\mathbf{x}}_1^q + (P_2^q)^{-1}\hat{\mathbf{x}}_2^q - \Gamma^{-1}\gamma\right) \tag{57}$$

The variables $\Gamma$ and $\gamma$ represents mutual covariance, and joint mean, is used to calculate the unknown correlation among the quantized estimates.

Here, we assumed only two estimates from sensor nodes is to be fused, but in practical multi-sensor and multi-target scenarios, there is a huge demand to track several targets simultaneously. In such cases, the CI method provides degraded fusion accuracy. To address this problem, the sampling covariance intersection (SCI) algorithm [33] is proposed to obtain the optimal-fused estimate in distributed fusion scenario.

#### 3) SAMPLING COVARIANCE INTERSECTION ALGORITHM

Let us assume that the $S$ number of covariances are fused to get fused covariance. This $S$ refers to individual tracks that are pertaining to the target. Using SCI method, the fused state estimate is as follows [33]

$$(\hat{\mathbf{x}}_f)_{SCI} = P\sum_{i=1}^{S}(P_i^q)^{-1}\hat{\mathbf{x}}_i^q \tag{58}$$

where, $P$ is calculated assuming that the tracks are independent, which is represented as

$$P^{-1} = \sum_{i=1}^{S}(P_i^q)^{-1} \tag{59}$$

The maximum and minimum range limits for fused covariance are calculated from the following

$$r_{\max} = \max_{j=1,2,3,\cdots,m}\frac{\hat{\mathbf{x}}_j' P^{-1}\hat{\mathbf{x}}_j}{\max\limits_{i=1,2,3,\cdots,S}\hat{\mathbf{x}}_j' P_i^{-1}\hat{\mathbf{x}}_j}, \tag{60}$$

and

$$r_{\min} = \min_{j=1,2,3,\cdots,m}\frac{\hat{\mathbf{x}}_j' P^{-1}\hat{\mathbf{x}}_j}{\min\limits_{i=1,2,3,\cdots,S}\hat{\mathbf{x}}_j' P_i^{-1}\hat{\mathbf{x}}_j}. \tag{61}$$

Here, $m$ refers to the number of random samples, $\mathbf{x}_j = \mathcal{N}(0,P_0);\ j=1,2,\cdots,m$.

Finally, the fused Covariance using SCI is given by

$$(P_f)_{SCI} = \frac{P}{ur_{min} + (1-u)r_{max}}, \tag{62}$$

where $u$ is optimal parameter, similar to $\omega$ in CI method, ranges from 0 to 1. The $r_{max}$ and $r_{min}$ are given in (60) and (61) respectively.

The algorithms like EI, CI, SCI perform well when error ellipses of individual sensors intersect [32]–[34]. Also, these algorithms calculate the fused estimate as an intersection of individual sensor error ellipsoids. However, in the case of individual sensor error ellipses that do not intersect, averaging techniques like linear and log-linear are utilized to get more conservative fusion results by compromising the minimum error covariance matrix [35], [36], [41]. Towards this end, this paper considers the AA fusion algorithm.

#### 4) ARITHMETIC Average(AA) FUSION

The fused state $(\hat{\mathbf{x}}_f)_{AA}$ using the arithmetic average is given by [41]

$$(\hat{\mathbf{x}}_f)_{AA} = \sum_{i=1}^{S} \omega_i \hat{\mathbf{x}}_i^q. \tag{63}$$

Similarly, the fused covariance $\left(P_f\right)_{AA}$ is represented as [41]

$$\left(P_f\right)_{AA} = \sum_{i=1}^{S} \omega_i \widetilde{P}_i^q, \tag{64}$$

where,

$$\widetilde{P}_i^q = P_i^q + \left((\hat{\mathbf{x}}_f)_{AA} - \hat{\mathbf{x}}_i^q\right)\left((\hat{\mathbf{x}}_f)_{AA} - \hat{\mathbf{x}}_i^q\right)'. \tag{65}$$

The weights in AA fusion technique [41] can be calculated by maximizing

$$\omega_i{}^* = \arg\max_{\omega_i} \left\{ \sum_{i=1}^{S} \omega_i \left[ tr\left((P_f)_{AA}^{-1} P_i\right) + \log \frac{\left|(P_f)_{AA}\right|}{|P_i|} + \left\|\hat{\mathbf{x}}_i - (\hat{\mathbf{x}}_i)_{AA}\right\|_{P_{AA}}^2 \right] \right\}, \tag{66}$$

where,

$$\left\|\hat{\mathbf{x}}_i - (\hat{\mathbf{x}}_i)_{AA}\right\|_{P_{AA}}^2 = \left(\hat{\mathbf{x}}_i - (\hat{\mathbf{x}}_i)_{AA}\right)(P_f)_{AA}^{-1}\left(\hat{\mathbf{x}}_i - (\hat{\mathbf{x}}_i)_{AA}\right)' \tag{67}$$

## V. RESULTS AND DISCUSSIONS

### A. SCENARIO GENERATION

A multi-sensor multi-target scenario in UWSN is considered for simulation. The sensors are assumed to be static, synchronous, and the maximum range of each sensor is $R_{\max} = 10000$m. The sensors receive range, and azimuth measurements of the targets present within the surveillance. The standard deviation of measurement noises corresponding to range and azimuth are $\sigma_r$ and $\sigma_\theta$ respectively. A clean environment (the false alarm density per unit volume is zero, and the target detection probability is unity) is considered for simulation. The locations of the sensors ($\{\mathbf{x}_i\}_{i=1}^S$), measurement noise standard deviations ($\sigma_r$ and $\sigma_\theta$), and sampling time ($\delta_t$) are given in Table 1.

All the targets follow the CV model. The target's starting positions and velocities in the surveillance are random, as shown in Fig. 3. The targets are starting at t = 1s and ends

**TABLE 1. Sensor parameters.**

| Sensor $i$ | Sensor location $\mathbf{x}_i$ (m) | $\sigma_r$ (m) | $\sigma_\theta$ (rad) | $\delta_t$ (s) |
|---|---|---|---|---|
| 1 | $[1000, 2000]'$ | 10 | 0.03 | 1 |
| 2 | $[4000, 6000]'$ | 10 | 0.03 | 1 |
| 3 | $[10000, 2000]'$ | 10 | 0.03 | 1 |
| 4 | $[10000, 6000]'$ | 10 | 0.03 | 1 |

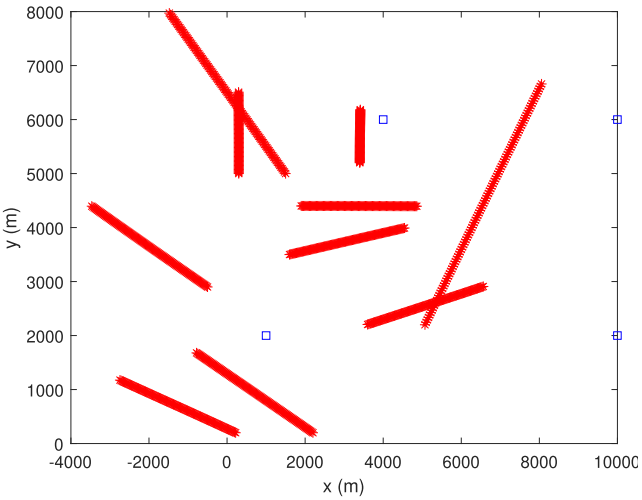


**FIGURE 3. Multi-sensor multi target scenario generation (red lines represent targets and blue squares denote sensors).**

at 100s with a sampling time of 1s, and follows CV model with

$$F = \begin{bmatrix} 1 & \delta_t & 0 & 0 \\ 0 & 1 & 0 & 0 \\ 0 & 0 & 1 & \delta_t \\ 0 & 0 & 0 & 0 \end{bmatrix}.$$

The target trajectory uncertainties like perturbations in the position and velocity are modeled as a process noise. The mean and standard deviations of the process noise vector are designated as

$$v = \begin{bmatrix} \mathcal{N}(0, 0.05) & \mathcal{N}(0, 0.02) & \mathcal{N}(0, 0.05) & \mathcal{N}(0, 0.02) \end{bmatrix},$$

where $\mathcal{N}(\cdot)$ represents Gaussian pdf.

### B. DESIGN PARAMETERS

Here, we used EKF with the GNN association. The tracks are initialized using the one-point initialization [42] by converting the obtained range and azimuth measurements. At $k = 1$, sensor report $r(1), \theta(1)$. These measurements are converted to Cartesian space as $x(1)$ and $y(1)$ is given by

$$x(1) = \lambda^{-1} r(1)\cos(\theta(1)) \quad \text{and}$$
$$y(1) = \lambda^{-1} r(1)\sin(\theta(1))$$

respectively. Here $\lambda = \exp\left(-\frac{\sigma_\theta^2}{2}\right)$. This unbiased conversion is valid for initialization, since it follows the necessary criteria of $\frac{r\sigma_\theta^2}{\sigma_r} \ll 0.4$ [43].

Therefore the initial state of the local tracker is

$$X(1) = \begin{bmatrix} x(1) & 0 & y(1) & 0 \end{bmatrix}.$$

Similarly, the initial covariance of the track is given by

$$P(1) = \begin{bmatrix} R_x & 0 & R_{xy} & 0 \\ 0 & (V_{max}/2)^2 & 0 & 0 \\ R_{xy} & 0 & R_y & 0 \\ 0 & 0 & 0 & (V_{max}/2)^2 \end{bmatrix},$$

where,

$$\begin{aligned} R_x &= (\lambda^{-2} - 2)\,(r(1))^2 \cos^2(\theta(1)) \\ &\quad + \frac{\left((r(1))^2 + \sigma_r^2\right)}{2}\left(1 + \lambda^4 \cos 2\theta(1)\right) \\ R_y &= (\lambda^{-2} - 2)\,(r(1))^2 \sin^2(\theta(1)) \\ &\quad + \frac{\left((r(1))^2 + \sigma_r^2\right)}{2}\left(1 - \lambda^4 \cos 2\theta(1)\right) \\ R_{xy} &= \left[\frac{\lambda^{-2}(r(1))^2}{2} + \frac{((r(1))^2 + \sigma_r^2)\lambda^4}{2} - ((r(1))^2\right] \sin 2\theta(1). \end{aligned}$$

Tracker assumes that the maximum velocity of the target is $V_{max} = 30$m/s. Moreover, the tunable parameters of process noise covariance and the measurement noise covariance of the filter are

$$\begin{aligned} Q &= \text{diag}([0.05^2, 0.02^2, 0.05^2, 0.02^2]) \quad \text{and} \\ R &= \text{diag}([10^2, 0.03^2]) \end{aligned}$$

respectively. The measurement validation is carried out using the gating technique, follows chi-square distribution $\chi_b^2(1 - t_p)$, where $b$ is the degree of freedom, and $t_p$ is the tail probability set to 0.05. The GNN association is solved by using the munkirs algorithm [44]. Moreover, the logic-based track maintenance [39] is utilized. We adopted the 7/10 and 4/10 rule for track confirmation and termination.

To perform the quantization, we choose three different step sizes. The low-step size is 5m, moderate-step size is 20m, and high-step size is 50m. For better understanding, we sweep the quantization step from low to high with a step size of 5m. Two different quantizations are used, namely linear and optimal. Linear quantization is based on uniform distribution [4], and optimal quantization is based on Lloyd's algorithm [5].

### C. TWO-SENSOR CASE

For the generated scenario, we considered two sensors, located at $\mathbf{x}_1, \mathbf{x}_2$ as given in Table 1. The local tracker provides state and covariance as local estimates. Once the quantization is performed on these state and covariance estimates, the quantized estimates are sent to the fusion center to obtain the fused estimate. Due to the independent behavior of sensors, the fusion center in distributed networks has inadequate information about the correlation among the sensors. This correlation information is needed to calculate the covariance region of the targets because of multiple sensors looking at each target. Due to the nonavailability of correlation (no correlation/unknown correlation) information, the overall tracking performance of the system diminishes.

EI, CI, and AA fusion methods have been used to find the fused state estimates. The EI uses the mutual information-based mean and covariance, which were derived using two initial estimates, to calculate the final fused mean and covariance [34]. On the other hand, CI uses trace or determinant minimization to calculate the fused covariance [32]. This minimization becomes a convex optimization problem. This nonlinear optimization was modeled as the well-known polynomial root-finding problem, allowing closed-form solutions to find the final fused covariance. The AA fusion method uses averaging technique to find the fused estimate [41].

#### 1) PRMSE ANALYSIS WITH MEDIUM-STEP SIZE

The position root mean square error (PRMSE) metric quantifies the results. This analysis considers medium-step size to perform both linear and optimal quantizations. The PRMSE for CI and EI for different quantizations concerning $k$ are plotted in Fig. 4a and Fig. 4b respectively. In the same Fig. 4, it is worth noting that we plotted the PRMSE without quantization case for comparison. It is observed that, for $k \in [1, 10]$, the PRMSE is significantly higher in both liner and optimal quantization cases, due to one point initialization. For linear quantization, after $k = 10$, we can observe that PRMSE is stable in between 16-18m in both EI and CI solutions. Simultaneously, the optimal quantization-based PRMSE is decreasing further. Even though we are using a medium-step size, we are attaining a huge difference in PRMSE values between linear & without quantization. The PRMSE of a fused estimate with linear quantization is nearly three times that of a fused estimate without quantization. The optimal Lloyd's based quantization [5] sets the quantization levels based on the received data samples. This implies that if more data samples are present over a specific range, Lloyd's quantizer opts for more quantization levels & vice versa. This is a massive advantage of using optimal quantization over linear quantization. For the same medium-step size, it is observed that the overall PRMSE of optimal quantization provides a two-fold improvement in tracking accuracy (optimal quantization PRMSE of 8.1415m and linear quantization PRMSE of 17.477m). The optimal quantization is offering 20% lower PRMSE compared to without applying the quantization method (without applying quantization PRMSE is 6.277m); hence both are in good agreement with each other. As $k$ increases in the optimal case, a smaller disparity between actual and estimated locations is observed. However, for the linear quantization method, the PRMSE is settling very fast at higher values. Further, the PRMSE of the quantized local estimates fused value using CI is higher than the EI approach. This is because unknown correlations are explicitly characterized before a fused value of the estimate is calculated; the EI approach is more accurate than the CI method.

In addition to CI and EI algorithms, the PRMSE corresponding to AA fusion technique is plotted in Fig. 5. Here, we can see that initially, the PRMSE is high and start diminishes similar to that of CI and EI algorithms. However, it is

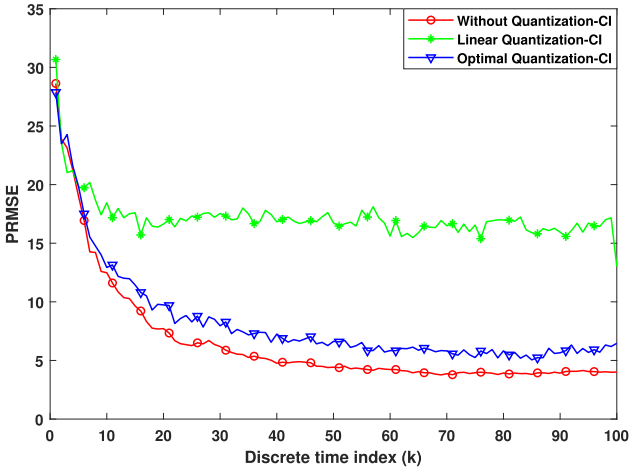


(a) CI

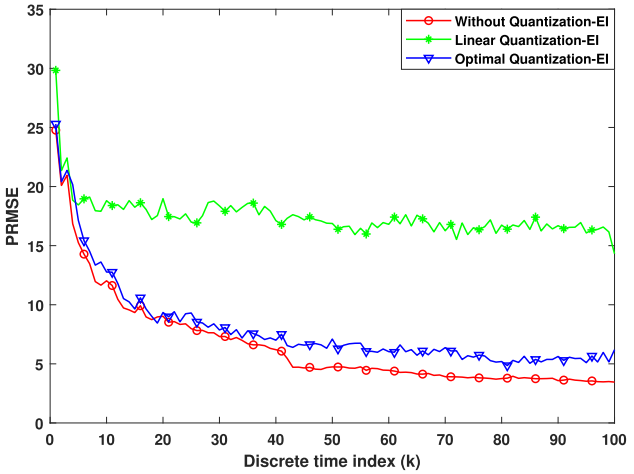


(b) EI

**FIGURE 4.** PRMSE of various fusion algorithms using linear, optimal, and without quantization.

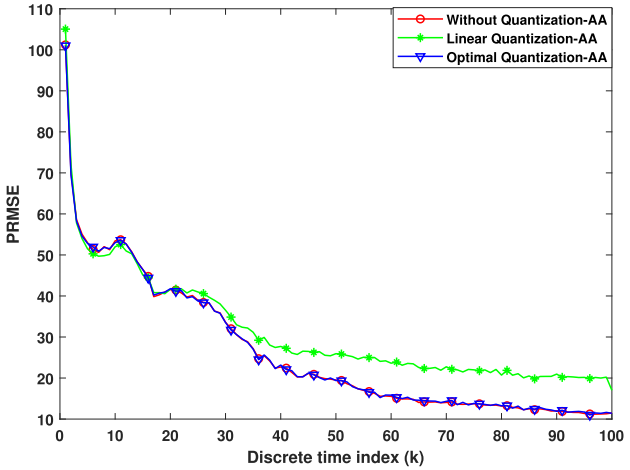


**FIGURE 5.** PRMSE of AA fusion algorithm using linear, optimal, and without quantization.

**TABLE 2.** PRMSE of fused quantized estimates with various quantization levels for two-sensor case.

| S.No. | $\nabla$ | $L$ | PRMSE | | | |
|---|---|---|---|---|---|---|
| | | | $Linear$ | $CI_{opt}$ | $EI_{opt}$ | $SCI_{opt}$ |
| 1 | 5 | 608 | 7.6559 | 6.6632 | 6.4593 | 6.4407 |
| 2 | 10 | 304 | 10.5490 | 7.0376 | 6.8464 | 6.8337 |
| 3 | 15 | 203 | 13.9576 | 7.5154 | 7.3539 | 7.3420 |
| 4 | 20 | 152 | 17.4770 | 8.2956 | 8.1484 | 8.1415 |
| 5 | 25 | 122 | 21.1955 | 9.0239 | 8.9169 | 8.9020 |
| 6 | 30 | 102 | 24.9235 | 10.2918 | 10.2266 | 10.1976 |
| 7 | 35 | 87 | 28.9262 | 12.3128 | 12.2789 | 12.2357 |
| 8 | 40 | 76 | 33.3026 | 13.7928 | 13.8071 | 13.7550 |
| 9 | 45 | 68 | 36.9676 | 15.3081 | 15.3664 | 15.3137 |
| 10 | 50 | 61 | 40.3824 | 16.4076 | 16.4875 | 16.4300 |
| without quantization | | | | 6.4998 | 6.5942 | 6.2770 |

worth noting that the PRMSE of AA fusion technique is higher than CI and EI fusion techniques. The simulation framework presented in this paper always has an intersection among the error ellipses of the local tracks. Hence, conservativeness is always guaranteed. For example, if the simulation results fails to get the intersection among the error ellipse of the local tracks, then the AA fusion technique yield same PRMSE values of EI and CI algorithms. From the Fig. 5, it is further observed that the PRMSE value of optimal quantization and without quantization are almost same. Whereas, the optimal quantization provides improved PRMSE compared to linear quantization in AA fusion technique.

### 2) PRMSE ANALYSIS BY SWEEPING STEP SIZE

To analyze the impact of quantization on local estimates, we varied the quantization step size ($\nabla$), the PRMSE values are calculated and tabulated in Table 2 along with quantization levels (L) for both linear and optimal quantization methods. In Table 2, $CI_{opt}$ refers to optimal quantization with CI fusion algorithm, and a similar representation is valid for others. If local estimates are linearly quantized, as we sweep the step size, there is a significant change in PRMSE. At the same time, if local estimates are non-linearly quantized, there is a slight difference in PRMSE values as we sweep the step size. All three fusion algorithms offer almost equal PRMSE for optimal quantization. We employed the SCI technique for the same case of two sensors and observed that it provides better-fused estimates than CI and EI. From Table 2, it is also observed that the difference in PRMSE of linear and optimal quantization is minimal if more quantization levels are employed (refer to step size of 5m and 10m). The low-step size optimal quantization offers almost the same PRMSE as that of without quantization (It can be seen from Fig. 6 that the optimal quantization provides a 97% accuracy with the assumption of without quantization gives 100% accuracy). In contrast, low-step size linear quantization offers 80% accuracy compared to without quantization. Which is same as that of the accuracy offered in the medium-step size case of optimal quantization. The same can be seen from Fig. 6 graphically.

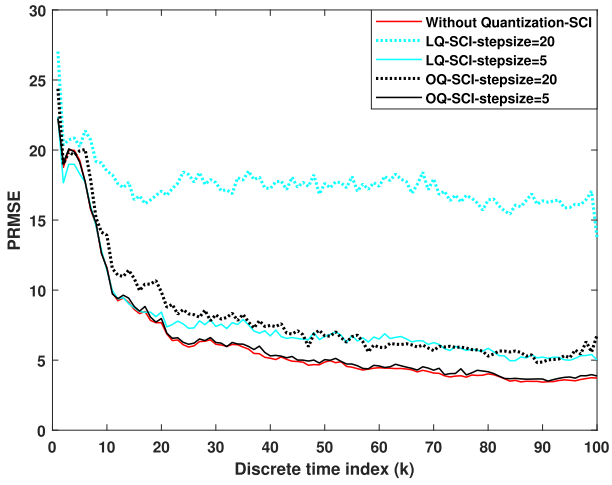


**FIGURE 6.** PRMSE of fused quantized estimates with medium-step and low-step quantization levels for two-sensor case.

### 3) BANDWIDTH ANALYSIS

In addition to PRMSE, the bandwidth required for each quantizer is considered as a metric of measure to compare the two different quantization methods. In general, for a binary communication system, a quantizer having $L$ quantized levels represents each input data sample using $n = \log_2(L)$ bits. Transferring the $m$ data samples will result in a $(m \times n)$ bps data rate, which in turn requires a minimum bandwidth equal to half the data rate. The number of quantization levels directly related to the number of bits to be transmitted determines bandwidth occupancy. For analysis, we kept the same step size for both uniform and optimal quantizations. It is observed from the Table-2 that, to achieve the same PRMSE using both linear and optimal quantization methods, the linear quantization requires 608 levels, whereas the optimal quantization requires 152 levels. Also, the same can be observed from Fig. 6 as well. To send the same data, linear quantizer requires $\log_2(608) \approx 10$ number of bits per level and optimal quantizer requires $\log_2(152) \approx 8$ number of bits per each level. Let us assume $m$ data samples are to be transmitted; Linear quantizer requires a bandwidth of $(10 \times m)/2 = (5 \times m)$bps whereas, optimal quantization requires $(8 \times m)/2 = (4 \times m)$bps. Therefore, the optimally quantized local estimates consume 20% lower bandwidth than the linear quantization method to achieve the same PRMSE.

### 4) ERROR ELLIPSE ANALYSIS

The correlation information among sensors is required to obtain the fused estimates in a multi-sensor scenario. But, no such information will be available in distributed fusion networks. As a consequence, deteriorated fused estimates are generated at the fusion center. To analyze the fused covariance estimate obtained using the different quantization methods, the error ellipses of the fused data are plotted in Figs. 7, 8, 9, and 10 for CI, EI, SCI, and AA, respectively, based on (53), (56), (62), and (64), respectively. The figures contain both linear and optimal quantizations along

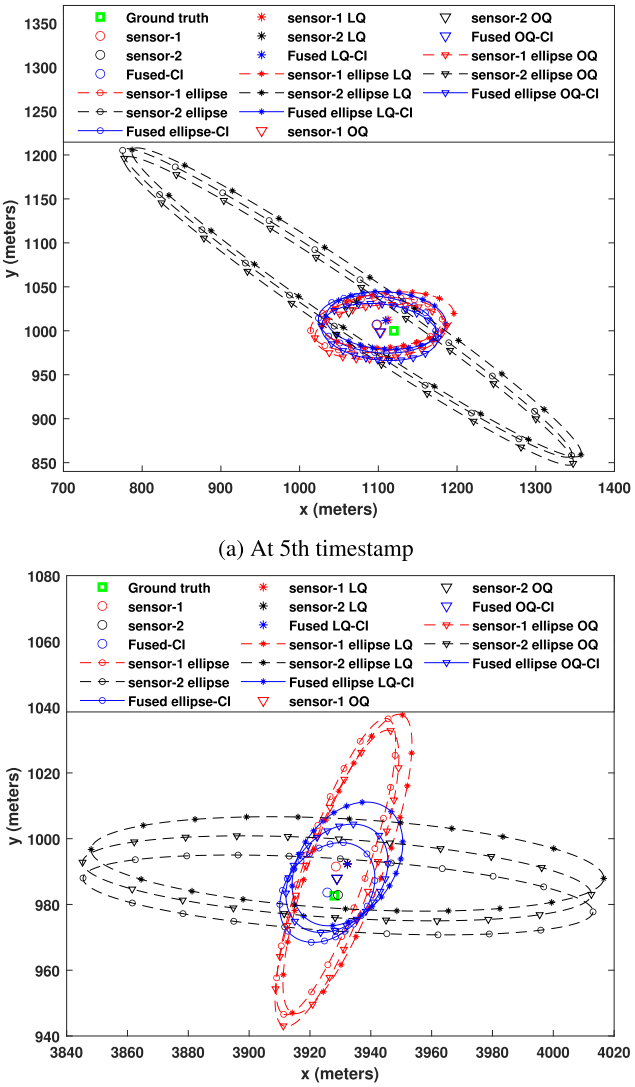


(a) At 5th timestamp

(b) At 99th timestamp

**FIGURE 7.** Error ellipses using CI fusion algorithm for two-sensor case.

with reported local tracks. The errors about each sensor are illustrated by the individual ellipsoids, representing the covariance region. The fused covariance ($P_f$) is smaller than the individual sensor covariance ($P_1^q$ and $P_2^q$) regions and is inside the intersection of the variances corresponding to the individual sensors. The optimization parameter in CI and SCI ($\omega$) provides a good fit for fused covariance. For simulation, we considered the optimization parameter ($\omega$) value as 0.5. However, for AA fusion, the fused covariance covers the major portions of the individual sensor covariance regions based on optimized fused weights, calculated using (66). The larger covariance is because of the fact that the consevativeness of AA fusion technique. Further, AA fusion technique ensures that, the true target falls within the fused covariance region irrespective of false and missed detections. In Fig.10a, the error ellipse is taken at $5^{th}$ time stamp and the fused

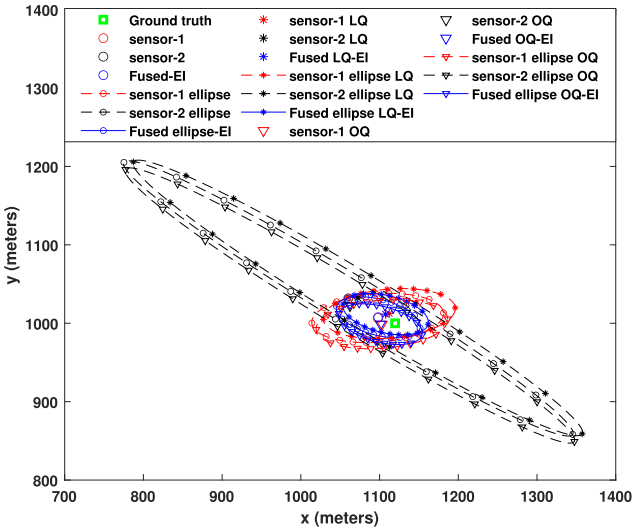


(a) At 5th timestamp

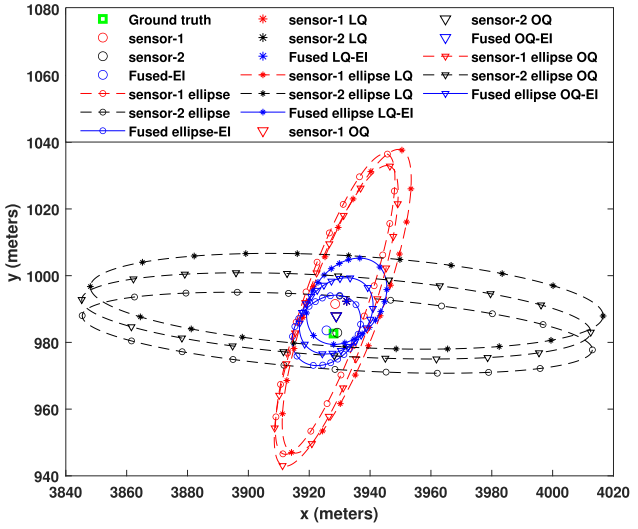


(b) At 99th timestamp

**FIGURE 8.** Error ellipses using EI fusion algorithm for two-sensor case.

covariance is almost equal to sensor-2 covariance, despite smaller covariance region provided by sensor-1. Similarly, the Fig.10b is taken at the $99^{th}$ time stamp, and it is observed that the fused covariance is larger compared to intersection region of the individual sensor covariance regions. The error ellipses for all fusion algorithms and individual sensors are plotted at $k = 5s$ and $k = 99s$, respectively. At $k = 5$, error ellipses are not settling and produce inaccurate fused results because of single point target initiation. The error ellipses at $k = 99$ provide improved fused covariance. The fused covariance region corresponding to linear quantization is slightly away from the ground truth value. On the other hand, the fused ellipse produced by all the local and optimally quantized estimates are nearer to the ground truth, which is also evident in Figs. 7, 8, and 9. A large covariance region is generated by the CI method owing to its over-conservativeness

**TABLE 3.** Computation time for various quantizations.

| S.No. | Type of quantization | Computation time (sec) |
|---|---|---|
| 1 | without quantization | 0.0192 |
| 2 | linear | 0.0402 |
| 3 | optimal | 0.1013 |

of covariance estimates [17]. Alternatively, the EI algorithm, which provides more accurate estimates than CI, limits the covariance region by explicitly analyzing the fusion with approximations. It is also observed that, the SCI offers better fused state and covariance estimates than the EI and CI based fusion methods.

#### 5) COMPUTATIONAL LOAD

Table 3 shows the computational time required in seconds to quantize and fuse the local estimates. The simulation time is calculated in MATLAB 2021a version with Intel(R) Xeon(R) E-2224G CPU 3.50GHz processor. The optimal quantization consumes five times more time than the without quantization technique to generate the fused one. In contrast, linear quantization technique requires twice the time compared to without quantization approach. Even though optimal quantization requires larger computational time, it consumes lesser bandwidth. It is also to be noted that the computational time is less than the sampling time of the sensor. Therefore, the algorithm is feasible for real-time applications.

### D. FOUR-SENSOR CASE

To further observe the influence of quantization of local state estimates in a multi-sensor scenario, a four-sensor case is considered by adding the two additional sensors to the two-sensor case. The static locations of the added sensors ($\mathbf{x}_3$ and $\mathbf{x}_4$) are mentioned in Table 1.

In contrast to the two-sensor case, here, the SCI and AA methods are used to fuse the associated tracks. Since the EI is limited to two sources, the CI is computationally demanding for more than two sources. The SCI first fuses the local track estimates with an assumption that they are independent. Thereafter, the covariance size of the fused track estimate is modified through a sampling process. In SCI, the fuser weight plays a critical role in estimating the mean. For a given unity fuser weight, the fuser is pessimistic. Whereas, for a zero fuser weight, the fuser is optimistic. The fuser weight equals to 0.5 provides the best consistency [33]. Henceforth, in this simulation, we considered the fuser weight as 0.5.

#### 1) PRMSE ANALYSIS

The analogy used in the two-sensor case is followed here with SCI fusion. The PRMSE for SCI with different quantization methods for medium and low step size is plotted in Fig. 11. For comparison, the PRMSE without the quantization case is also plotted in Fig. 11. It is observed that the PRMSE of a fused estimate with linear quantization is nearly four times that of a fused estimate without quantization. For the same medium-step size, it is observed that the overall PRMSE of

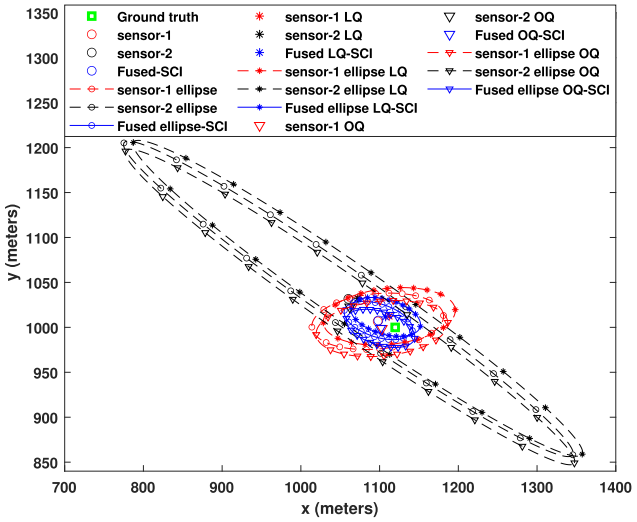


(a) At 5th timestamp

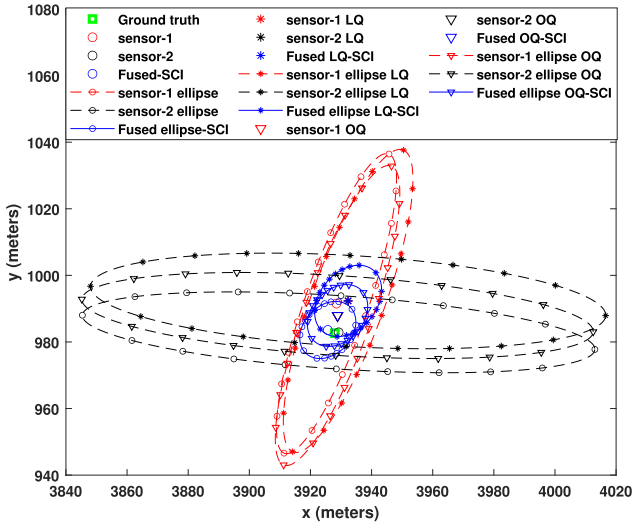


(b) At 99th timestamp

**FIGURE 9.** Error ellipses using SCI fusion algorithm for two-sensor case.

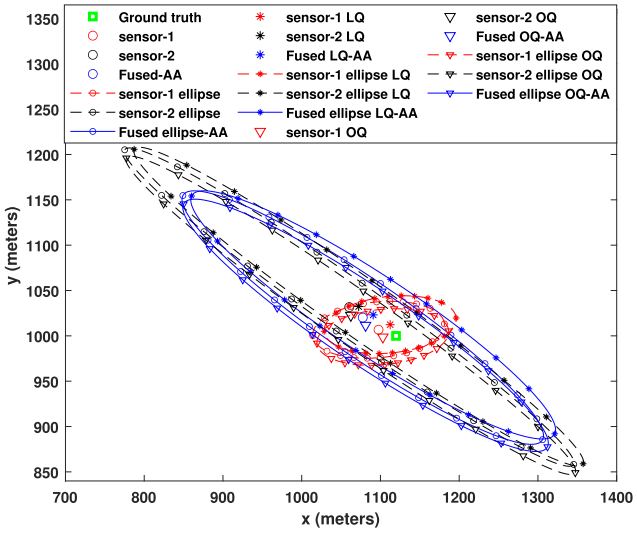


(a) At 5th timestamp

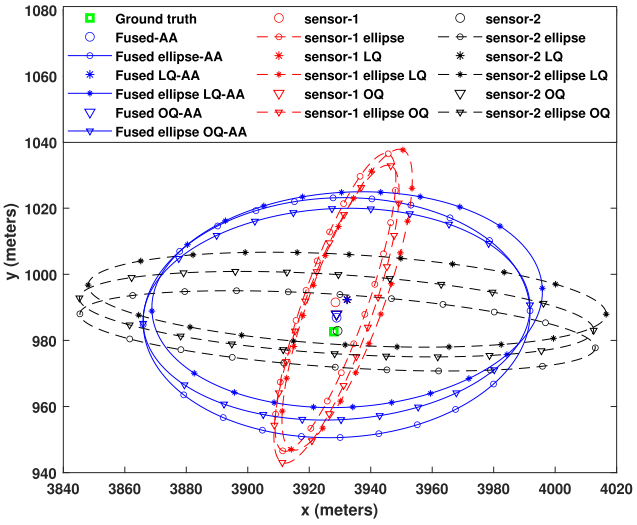


(b) At 99th timestamp

**FIGURE 10.** Error ellipses using AA fusion algorithm for two-sensor case.

optimal quantization provides a three-fold improvement in tracking accuracy (optimal quantization PRMSE is 6.5453m and linear quantization PRMSE is 20.1704m). The optimal quantization offers 35% lesser accuracy than without considering the quantization, which offers a PRMSE value of 4.1766m; hence, both are in good agreement with each other. At the same time, linear quantization offers 80% lesser accuracy than without applying the quantization method. As $k$ increases, the optimal quantization method observed a smaller disparity between actual and estimated locations. As in the two-sensor case, the PRMSE follows the same trend for both quantization methods. The optimally quantized estimates provide improved PRMSE compared to uniform quantization. The quantized local estimates give more accuracy than the two-sensor case because of the increased number of sensors in surveillance. Thus, the presence of more sensors provides a large number of local state estimates, which in turn improves the accuracy of the fused state estimate.

In order to further analyze the effect of quantization, the step size is increased from 5 to 50m with 5m increment at each step, the PRMSE values for fused state estimates are tabulated in Table 4. The low-step size optimal quantization offers almost the same PRMSE as that of without quantization (it is evident from Fig. 11 that optimal quantization provides 97% accuracy with the assumption that without quantization yields 100% accuracy). Whereas, low-step size linear quantization offers 67% accuracy compared to without quantization. For high-step size, the PRMSE offered by linear quantization is ten times that of the unquantized value. Alternatively, optimal quantization provides three times that of the unquantized value. The PRMSE values reveal that, even though fewer quantization levels are considered, the optimal

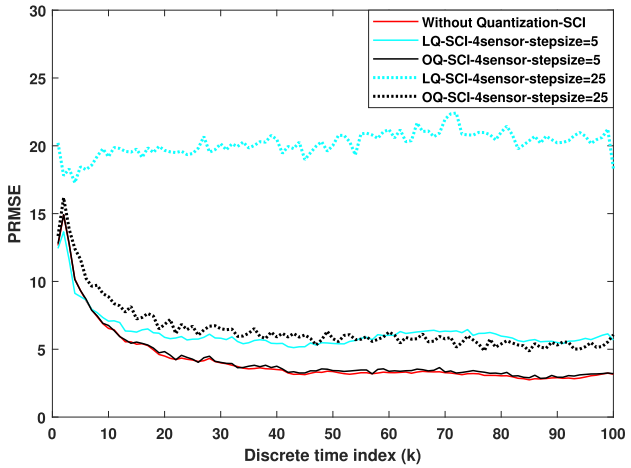


**FIGURE 11.** PRMSE of fused quantized estimates with medium-step and low-step quantization levels for four-sensor case.

**TABLE 4.** PRMSE of SCI fused quantized estimates with various quantization levels for four-sensor case.

| S.No. | $\nabla$ | $L$ | PRMSE | |
|---|---|---|---|---|
| | | | Linear | Optimal |
| 1 | 5 | 631 | 6.2241 | 4.2974 |
| 2 | 10 | 316 | 9.3556 | 4.6534 |
| 3 | 15 | 211 | 12.8038 | 5.2326 |
| 4 | 20 | 158 | 16.4145 | 5.9206 |
| 5 | 25 | 127 | 20.1704 | 6.5453 |
| 6 | 30 | 106 | 24.1033 | 7.5457 |
| 7 | 35 | 91 | 27.4943 | 9.2260 |
| 8 | 40 | 79 | 31.3686 | 10.6945 |
| 9 | 45 | 71 | 35.5195 | 11.9162 |
| 10 | 50 | 64 | 39.1156 | 13.1600 |
| without quantization | | | 4.1766 | 4.1766 |

quantization method provides superior performance than the linear one.

### 2) BANDWIDTH ANALYSIS

From Table 4, it is observed that, to achieve the same PRMSE value of 6.3m, linear quantization requires 631 levels, whereas optimal Lloyd's approach requires only 127 levels, and the corresponding PRMSEs are plotted in Fig. 11. In terms of the number of bits, a linear quantizer requires $\log_2(631) \approx 10$ bits to represent each quantization level, and an optimal quantizer requires $\log_2(127) \approx 7$ bits. So, the bandwidth required to send $m$ samples with linear quantizer is $(5 \times m)$bps, and it is $(3.5 \times m)$bps for optimal quantizer. Therefore, the linear quantizer occupies 42% of higher bandwidth than the optimal quantizer. Also, the reduction in PRMSE for the four-sensor case is significant compared to the two-sensor case when optimum quantization is adopted. However, it is quite small when linear quantization is adopted.

### 3) ERROR ELLIPSE ANALYSIS

To analyze the fused covariance estimate, the error ellipses are drawn for the individual sensors. The error ellipses are

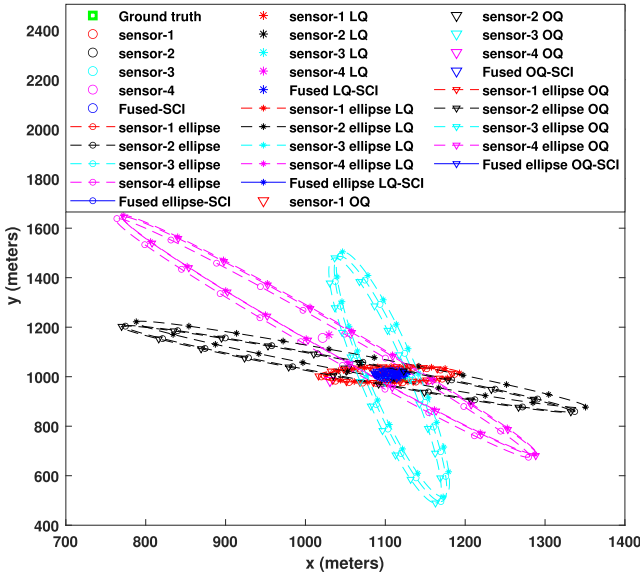


(a) At 5th timestamp

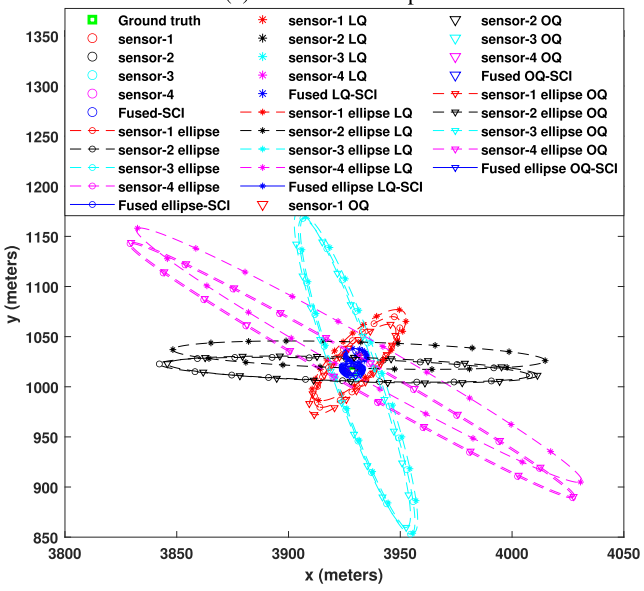


(b) At 99th timestamp

**FIGURE 12.** Error ellipses using SCI fusion algorithm for four-sensor case.

plotted at initial and final timestamps of 5s and 99s. The fused covariance region in SCI is defined as the intersection space of ellipsoids from all sensors. In AA, the fused covariance region is the arithmetic average of individual sensor ellipsoids. These are depicted in Fig. 12 and 13 respectively. The covariance region in SCI is diminished compared to the two-sensor case because of more sensors. This provides an accurate and exact region of fused covariance, and moreover, it encircles the ground truth. This states that SCI fusion with quantized local estimates achieves enhanced performance. However, the covariance region in AA is increased for four-sensor case compared to two-sensor owing to its over conservative property.

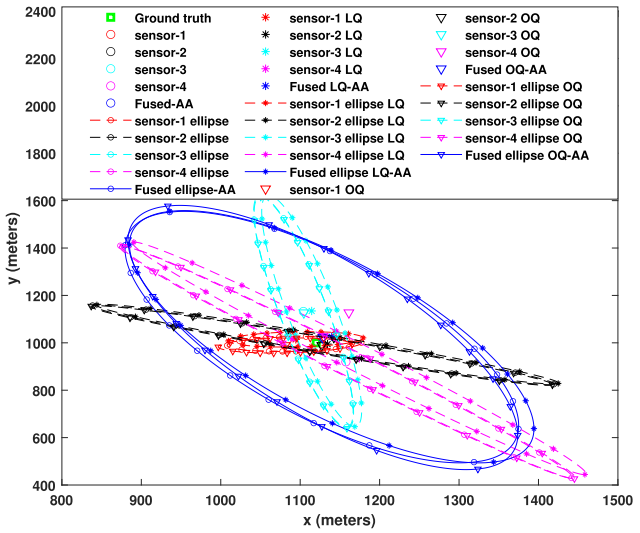


(a) At 5th timestamp

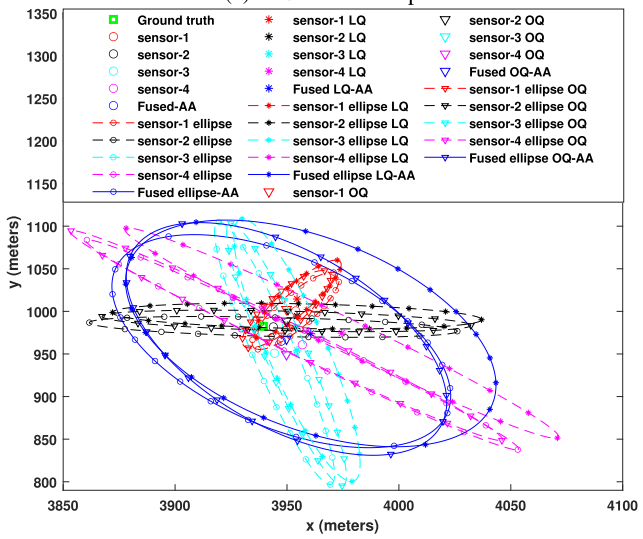


(b) At 99th timestamp

**FIGURE 13.** Error ellipses using AA fusion algorithm for four-sensor case.

## VI. CONCLUSION

This paper presents state quantization instead of measurement quantization due to its real-time feasibility and linear relationship. We propose to use state quantization in distributed tracking followed by fusion as an alternative solution to measurement quantization followed by centralized tracking. The local tracker uses the EKF and GNN association framework to estimate the updated state and covariance of the time-varying targets. Besides, linear and optimal quantization schemes are explored to quantize the densely available local estimates to feed the fusion node. Further, S-D assignment-based T2TA is performed at the fusion center to identify the correlated tracks that pertain to the same target from the available quantized local tracks. The associated tracks are fused using correlation-free fusion algorithms, namely ellipsoid intersection (EI), covariance intersection (CI), modified covariance intersection (SCI), and arithmetic average (AA) fusion methods. In addition, two different cases (two-sensor and four-sensor case) are analyzed for distributed UWSNs. The fused quantized local tracks are quantified using PRMSE, bandwidth, and error ellipse metrics. The simulation results demonstrates that, applying the optimal quantization over linear quantization provides improved bandwidth efficiency for multi sensor case. The optimal quantization consumes 20% and 30% lesser bandwidth compared to linear quantization for two and four sensor cases respectively. Further, optimal quantization yields improved PRMSE values compared to linear quantization for both two and four sensor cases. Furthermore, optimal quantization provides comparable performance as that of the unquantized scenario for both the cases that are investigated in this study.

## REFERENCES


[1] J. Luo, Y. Han, and L. Fan, "Underwater acoustic target tracking: A review," *Sensors*, vol. 18, no. 1, p. 112, Jan. 2018.

[2] S. Fattah, A. Gani, I. Ahmedy, M. Y. I. Idris, and I. A. Targio Hashem, "A survey on underwater wireless sensor networks: Requirements, taxonomy, recent advances, and open research challenges," *Sensors*, vol. 20, no. 18, p. 5393, 2020.

[3] E. Felemban, F. K. Shaikh, U. M. Qureshi, A. A. Sheikh, and S. B. Qaisar, "Underwater sensor network applications: A comprehensive survey," *Int. J. Distrib. Sensor Netw.*, vol. 11, no. 11, Nov. 2015, Art. no. 896832.

[4] E. A. Lee and D. G. Messerschmitt, *Digital Communication*. New York, NY, USA: Springer, 2012.

[5] S. Lloyd, "Least squares quantization in PCM," *IEEE Trans. Inf. Theory*, vol. 28, no. 2, pp. 129–137, Mar. 1982.

[6] E. J. Msechu and G. B. Giannakis, "Sensor-centric data reduction for estimation with WSNs via censoring and quantization," *IEEE Trans. Signal Process.*, vol. 60, no. 1, pp. 400–414, Jan. 2012.

[7] H. Li, "Distributed adaptive quantization and estimation for wireless sensor networks," in *Proc. IEEE Int. Conf. Acoust., Speech Signal Process. (ICASSP)*, vol. 3, Apr. 2007, pp. III–533.

[8] X. Luo and G. B. Giannakis, "Energy-constrained optimal quantization for wireless sensor networks," *EURASIP J. Adv. Signal Process.*, vol. 2008, no. 1, pp. 1–12, Dec. 2007.

[9] L. D. Stone and S. L. Anderson, "Multiple target tracking with quantized measurements: A standard Bayesian approach," in *Proc. 17th Int. Conf. Inf. Fusion (FUSION)*, Jul. 2014, pp. 1–8.

[10] Z. Duan, V. P. Jilkov, and X. R. Li, "State estimation with quantized measurements: Approximate MMSE approach," in *Proc. 11th Int. Conf. Inf. Fusion*, Jun./Jul. 2008, pp. 1–6.

[11] S. Zhang, H. Chen, M. Liu, and Q. Zhang, "Optimal quantization scheme for data-efficient target tracking via UWSNs using quantized measurements," *Sensors*, vol. 17, no. 11, p. 2565, Nov. 2017.

[12] Y. Zhou, J. Li, and D. Wang, "Target tracking in wireless sensor networks using adaptive measurement quantization," *Sci. China Inf. Sci.*, vol. 55, no. 4, pp. 827–838, Apr. 2012.

[13] P. Qian, Y. Guo, N. Li, and S. Yang, "Variational Bayesian inference-based multiple target localization in WSNs with quantized received signal strength," *IEEE Access*, vol. 7, pp. 60228–60241, 2019.

[14] J. Luo, Y. Han, and X. He, "Optimal bit allocation for maneuvering target tracking in UWSNs with additive and multiplicative noise," *Signal Process.*, vol. 164, pp. 125–135, Nov. 2019.

[15] H. Sun, X. Wang, K. Yang, and T. Peng, "Analysis of distributed wireless sensor systems with a switched quantizer," *Complexity*, vol. 2021, pp. 1–14, Jul. 2021.

[16] Y. Bar-Shalom, X. R. Li, and T. Kirubarajan, *Estimation With Applications to Tracking and Navigation: Theory Algorithms and Software*. Hoboken, NJ, USA: Wiley, 2004.

[17] Y. Bar-Shalom, P. K. Willett, and X. Tian, *Tracking Data Fusion*, vol. 11. Storrs, CT, USA:, YBS, 2011.

[18] A. Sinha, Z. Ding, T. Kirubarajan, and M. Farooq, "Track quality based multitarget tracking approach for global nearest-neighbor association," *IEEE Trans. Aerosp. Electron. Syst.*, vol. 48, no. 2, pp. 1179–1191, Apr. 2012.

[19] Y. Bar-Shalom, F. Daum, and J. Huang, "The probabilistic data association filter," *IEEE Control Syst.*, vol. 29, no. 6, pp. 82–100, Dec. 2009.
[20] S. S. Blackman, "Multiple hypothesis tracking for multiple target tracking," *IEEE Aerosp. Electron. Syst. Mag.*, vol. 19, no. 1, pp. 5–18, Jan. 2004.
[21] X. Jiang, K. Harishan, R. Tharmarasa, T. Kirubarajan, and T. Thayaparan, "Integrated track initialization and maintenance in heavy clutter using probabilistic data association," *Signal Process.*, vol. 94, pp. 241–250, Jan. 2014.
[22] M. P. Muresan, S. Nedevschi, and R. Danescu, "Robust data association using fusion of data-driven and engineered features for real-time pedestrian tracking in thermal images," *Sensors*, vol. 21, no. 23, p. 8005, Nov. 2021.
[23] S. Jiayao, S. Zhou, Y. Cui, and Z. Fang, "Real-time 3D single object tracking with transformer," *IEEE Trans. Multimedia*, early access, Jan. 27, 2022, doi: 10.1109/TMM.2022.3146714.
[24] Y. Bar-Shalom, "On the track-to-track correlation problem," *IEEE Trans. Autom. Control*, vol. 26, no. 2, pp. 571–572, Apr. 1981.
[25] Z. Liu, G. Xiao, H. Liu, and H. Wei, "Multi-sensor measurement and data fusion," *IEEE Instrum. Meas. Mag.*, vol. 25, no. 1, pp. 28–36, Feb. 2022.
[26] D. L. Hall and J. Llinas, "An introduction to multisensor data fusion," *Proc. IEEE*, vol. 85, no. 1, pp. 6–23, Jan. 1997.
[27] B. Khaleghi, A. Khamis, F. O. Karray, and S. N. Razavi, "Multisensor data fusion: A review of the state-of-the-art," *Inf. Fusion*, vol. 14, no. 1, pp. 28–44, Jan. 2013.
[28] N. Shaukat, A. Ali, M. Javed Iqbal, M. Moinuddin, and P. Otero, "Multi-sensor fusion for underwater vehicle localization by augmentation of RBF neural network and error-state Kalman filter," *Sensors*, vol. 21, no. 4, p. 1149, Feb. 2021.
[29] M. E. Liggins, C.-Y. Chong, I. Kadar, M. G. Alford, V. Vannicola, and S. Thomopoulos, "Distributed fusion architectures and algorithms for target tracking," *Proc. IEEE*, vol. 85, no. 1, pp. 95–107, Jan. 1997.
[30] S. Duncan and S. Sameer, "Approaches to multisensor data fusion in target tracking: A survey," *IEEE Trans. Knowl. Data Eng.*, vol. 18, no. 12, pp. 1696–1710, Dec. 2006.
[31] M. A. Bakr and S. Lee, "Distributed multisensor data fusion under unknown correlation and data inconsistency," *Sensors*, vol. 17, no. 11, p. 2472, Oct. 2017.
[32] S. J. Julier and J. K. Uhlmann, "A non-divergent estimation algorithm in the presence of unknown correlations," in *Proc. Amer. Control Conf.*, vol. 4, Jun. 1997, pp. 2369–2373.
[33] X. Tian, Y. Bar-Shalom, and G. Chen, "A no-loss covariance intersection algorithm for track-to-track fusion," *Proc. SPIE*, vol. 7698, Apr. 2010, Art. no. 76980S.
[34] J. Sijs and M. Lazar, "State fusion with unknown correlation: Ellipsoidal intersection," *Automatica*, vol. 48, no. 8, pp. 1874–1878, Aug. 2012.
[35] T. Li, H. Fan, J. Garcia, and J. M. Corchado, "Second-order statistics analysis and comparison between arithmetic and geometric average fusion: Application to multi-sensor target tracking," *Inf. Fusion*, vol. 51, pp. 233–243, Nov. 2019.
[36] B. Noack, J. Sijs, M. Reinhardt, and U. D. Hanebeck, "Decentralized data fusion with inverse covariance intersection," *Automatica*, vol. 79, pp. 35–41, May 2017.
[37] Y. Wang, X. Wang, Y. Shan, and N. Cui, "Quantized genetic resampling particle filtering for vision-based ground moving target tracking," *Aerosp. Sci. Technol.*, vol. 103, Aug. 2020, Art. no. 105925.
[38] R. B. N. Balarami, S. Gunnery, P. Bethi, and S. Pathipati, "Quantized directional cosine measurements based localization," in *Proc. 10th IEEE Int. Conf. Commun. Syst. Netw. Technol. (CSNT)*, Jun. 2021, pp. 99–104.
[39] X. Jiang, K. Harishan, R. Tharmarasa, T. Kirubarajan, and T. Thayaparan, "Integrated track initialization and maintenance in heavy clutter using probabilistic data association," *Signal Process.*, vol. 94, pp. 241–250, Jan. 2014.
[40] M. Reinhardt, B. Noack, and U. D. Hanebeck, "Closed-form optimization of covariance intersection for low-dimensional matrices," in *Proc. 15th Int. Conf. Inf. Fusion*, Jul. 2012, pp. 1891–1896.
[41] T. Li, Y. Xin, Y. Song, E. Song, and H. Fan, "Some statistic and information-theoretic results on arithmetic average density fusion," 2021, *arXiv:2110.01440*.
[42] D. Musicki and T. L. Song, "Track initialization: Prior target velocity and acceleration moments," *IEEE Trans. Aerosp. Electron. Syst.*, vol. 49, no. 1, pp. 665–670, Jan. 2013.
[43] M. Longbin, S. Xiaoquan, Z. Yiyu, S. Z. Kang, and Y. Bar-Shalom, "Unbiased converted measurements for tracking," *IEEE Trans. Aerosp. Electron. Syst.*, vol. 34, no. 3, pp. 1023–1027, Jul. 1998.
[44] S. S. Blackman and R. Popoli, *Design and Analysis of Modern Tracking Systems*. Boston, MA, USA: Artech House, 1999.

**B. N. BALARAMI REDDY** (Graduate Student Member, IEEE) received the master's degree in microwave and communication engineering from Jawaharlal Nehru Technological University, Kakinada, Andhra Pradesh, India. He is currently pursuing the Ph.D. degree with the National Institute of Technology Karnataka, India. His research interests include target tracking and flexible/wearable antennas for wireless body area networks.

**BETHI PARDHASARADHI** received the B.Tech. degree in electronics and communication engineering from Jawaharlal Nehru Technological University, Kakinada (JNTU-K), Andhra Pradesh, India, in 2014, and the M.Tech. degree in VLSI design from the Indian Institute of Information Technology and Management, Gwalior (IIITM), Madya Pradesh, India, in 2016. He is currently pursuing the full-time Ph.D. degree with the National Institute of Technology Karnataka (NIT-K), Surathkal, India. He was a recipient of Sir C. V. Raman Award from the Institution of Engineering and Technology (IET) for outstanding academics and research. He was a Visiting Ph.D. Scholar with the ETF Laboratory, McMaster University, Canada, under the supervision of Prof. T. Kirubarajan, in 2018 and 2019. His research interests include intentional interference in navigation, target tracking, and information fusion.

**GUNNERY SRINATH** (Graduate Student Member, IEEE) received the B.Tech. degree in electronics and communication engineering from Jawaharlal Nehru Technological University, Anantapur, India, in 2013, and the M.Tech. degree in digital communication from ABV-IIITM, Gwalior, India, in 2016. He is currently pursuing the Ph.D. degree in electronics and communication engineering with the National Institute of Technology Karnataka Surathkal, Mangalore, India. From 2018 to 2019, he was a Visiting Ph.D. Student with the Estimation, Tracking and Fusion Research Laboratory, McMaster University, Hamilton, ON, Canada. His research interests include cognitive radio, radar signal processing, radar and communication system spectrum sharing, and target tracking.

**PATHIPATI SRIHARI** (Senior Member, IEEE) received the B.Tech. degree in electronics and communication engineering from Sri Venkateswara University, the master's degree in communications engineering and signal processing from the University of Plymouth, England, U.K., and the Ph.D. degree in the field of radar signal processing from Andhra University, in 2012. He is currently working as an Assistant Professor with the National Institute of Technology Karnataka, Surathkal, India. He worked as a Visiting Assistant Professor with McMaster University, Canada, in 2014. He received 2010 IEEE Asia Pacific Outstanding Branch Counselor Award. He is a Senior Member of ACM. He is a fellow of IETE and a member of IEICE, Japan. He received the Young Scientist Award from the Department of Science and Technology (DST), New Delhi to carryout sponsored research project entitled development of efficient target tracking algorithms in the presence of ECM. His research interests include radar target tracking, radar waveform design, and efficient DSP algorithms for radar applications.